ATRAZINE ADSORPTION AT THE AIR/SILICA INTERFACE

A Thesis

Presented in Partial Fulfillment of the Requirements for

the Degree Master of Science

in the Graduate School of The Ohio State University

By

Nadia Ninel Casillas Ituarte

*****

The Ohio State University
2005

Master's Examination Committee:

Dr. Heather C. Allen, Adviser

Dr. Linda Weavers

Dr. Yu-Ping Chin

Approved by

_____

Adviser
Environmental Science Graduate Program

ABSTRACT

Sorption-desorption processes of pesticides on clay minerals strongly influence the fate of pesticides in soil environments. Soils are heterogeneous mixtures and there are many interrelated factors that play important roles in the sorption process. In order to elucidate the binding mechanism between an herbicide and a soil constituent, model systems have been used. Atrazine [6-chloro-N^2-ethyl-N^4-isopropyl-1,3,5-triazine-2,4-diamine], one of the most common members of the *s*-triazine herbicide family has been detected in ground and surface waters, and in precipitation. Despite the extensive work available on the atrazine sorption process, little is known at the molecular level about the interactions of atrazine with clays.

A surface-selective, technique sum frequency generation (SFG) spectroscopy, is used in this study to examine the air-solid interface of atrazine on silica, providing detailed, molecular information about the distribution of this herbicide at the silica surface. Atrazine interacts with the surface of silica through hydrogen bonding of the amine moieties and the silanol OH groups. This weak bonding interaction suggests that atrazine, once adsorbed onto the clay fraction of soils, is easily desorbed. It can then be transported deeper into the soils, and ultimately into the ground water. This proposed

hydrogen bonding mechanism is consistent with previous studies of atrazine sorption on clay minerals.

ACKNOWLEDGMENTS

I would like to thank my adviser, Heather Allen, for providing support and encouragement to accomplish the research for this degree.

I would also like to thank all of the members of the Allen lab. In particular, Dr. Dingfang Liu, Dr. Gang Ma, and Dr. Laura Voss for their technical guidance, Lisa Van Loon for correcting my English and providing ideas to the improvement of this thesis work.

I whish to thank Dr. Sandhya Gopalakrishnan for all her generous assistance to strengthen the discussion.

I also whish to thank Roxana Sierra my friend and accomplice through this journey.

I especially want to thank my parents for their constant encouragement and support to achieve all my goals.

This research was partially supported by National Council of Science and Technology of Mexico (CONACYT)

VITA

April 27, 1978. . . . . .Born – Delicias Chih., Mexico

2000. . . . . B.S. Bacteriologist Parasitologist Chemist
Autonomous University of Chihuahua, Mexico

2002 – 2005. . . . . Graduate Teaching and Research Assistant
The Ohio State University

FIELDS OF STUDY

Major Field: Environmental Sciences

TABLE OF CONTENTS

LIST OF TABLES

LIST OF FIGURES

LIST OF ABBREVIATIONS

NMR	nuclear magnetic resonance
IR	infrared
EPA	Environmental Protection Agency
CCD	charge coupled device
ha	hectare
mg	milligram
ºC	degrees Celsius
UV	ultraviolet
L	liter
m	mili
μ	micro
E	electric field
g	gram
n	nano
M	moles per liter
OPA/OPG	optical parametric generator/amplifier
ps	picosecond

min	minute
β	beta – molecular susceptibility
χ	chi – macroscopic second-order nonlinear susceptibility
Γ	gamma – half-width at half-maximum
cm^{-1}	wavenumber
Hz	hertz
NIST	National Institute of Standards and Technology

CHAPTER 1

INTRODUCTION

The fate of herbicides in soil, and surface and ground waters is determined by several factors including retention, transformation, and transport processes. Sorption-desorption processes are the primary method for retention of herbicides on soil constituents and can exert control over the transformation, transport and biological effects of herbicides in the environment. (Davies E., and Jabeen N., 2003, Lesan H., Bhandari A., 2003) The phytotoxicity and selectivity of herbicides, their effect on non-target organisms, and the risk of surface and ground water contamination are affected by the distribution of the herbicide between the liquid or gas phase and the adsorbed phase. (Calvet R., 1980) Under most conditions herbicides are adsorbed on both organic and inorganic soil fractions. (Laird D., *et al* 1992) It is well established that the retention of herbicides is strongly correlated to the organic fraction content and that inorganic constituents play a comparatively minor role. (Karickhoff S., *et al* 1979, Chiou C., *et al* 1979, Hasset J., *et al* 1981, Barriuso E., *et al* 1992) However, in particular herbicide categories such as triazines and carbamates the retention by inorganic fraction may equal or exceed that by organic fraction, based on the estimates of sorption by the isolated sorbents. (Laird D., *et al* 1992, Sawhney B. and Singh S., 1997, Sheng G., *et al* 2001, Li H., *et al* 2003)

To elucidate the binding mechanisms responsible for the interactions between an herbicide and a soil constituent, it is important to study the sorption behavior on the relevant soil component. Since soils are heterogeneous mixtures, the study of these interactions is complicated because there are many interrelated factors that play important roles in the behavior of both sorbents and sorbates. (Sposito G., 1994, Myneni S., 2002) Therefore it is necessary to study the interaction between sorbate molecules and soil mineral particles by using model systems.

Clay minerals constitute the last barrier to a translocation of environmental chemicals by soil leachates into ground water. (Davies E., and Jabeen N., 2003) As a result clay minerals and organic matter are considered the most important soil constituents of the adsorption process. (Worrall F., *et al* 1996, Clausen L., *et al* 2001) Due to its stability and its ubiquitous nature (it is considered a major component in the earth's crust), silica, SiO_2, constitutes the major portion of all sand and silt fraction, and is also the major component of the coarse clay fraction of many soils. (Dixon J., and Weed S., 1989) Silica occurs as seven distinct polymorphs including both crystal and amorphous forms. Quartz is recognized as the most stable and abundant form in the soil environment. (Dixon J., and Weed S., 1989)

In the soil environment, the silica surface is fully hydroxylated. (Langmuir D., 1997, Stumm W., and Morgan J., 1996) Depending on the relative humidity there are a number of monolayers of water molecules adsorbed on the hydroxylated surface due to the hydration of the SiO_2 surface. (Iler R., 1979) The presence of OH groups on the silica

surface has been investigated by spectral and chemical analysis. (Morrow B., and McFarlan A., 1990, Zhuravlev L., 2000) The surface OH groups act as adsorption sites for adsorbates capable of undergoing donor-acceptor interactions. Thus, surface silanol groups play a key role in sorption processes involving physical bonding forces (van der Waals or electrostatic interactions, hydrogen bonding, dipole-dipole interactions) and chemical bonding forces. Sorbate molecules bound through chemisorption are different chemical entities than those bound through physisorption.

Three different types of surface silanol OH have been described: (1) Isolated single silanol OH groups (≡SiOH); (2) Geminal silanol OH groups (=$Si(OH)_2$); (3) Vicinal silanol OH groups (OH group bound through hydrogen bonds) (Figure 1.1). (Zhuravlev L., 2000)

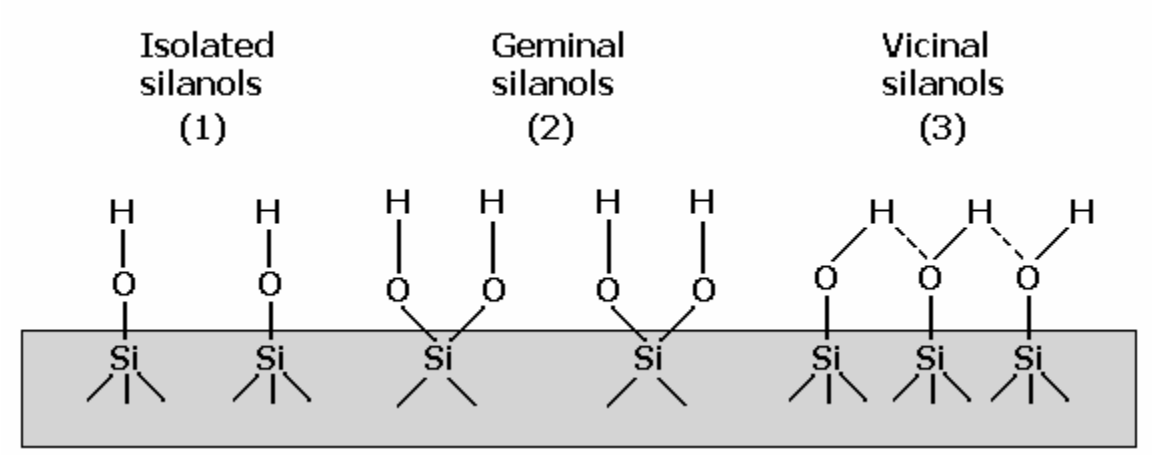

Figure 1.1 Surface silanol OH groups at the at the silica surface; (1) isolated silanol OH groups, (2) geminal silanol OH groups, and (3) vicinal silanol OH groups. Adapted from Zhuravlev L, 2000.

The surface charge of a mineral surface is the consequence of the protonation-deprotonation of surface functional groups (mostly OH). Numerous experimental studies have been devoted to measuring silica surface charge using different techniques including potentiometric titrations, NMR, IR and X-ray photoelectron spectroscopy. (Li H., and de Bruyn P., 1966, Tuel A., *et al* 1990, Van Roosmalen A.J. and Legrand A., 1990, Cardenas J., 2004, Duval Y. *et al* 2002)

In the analysis of the surface charge by X-ray photoelectron spectroscopy the pKa values obtained are:

$$\equiv SiOH_2^+ \rightarrow \equiv SiOH + H^+ \qquad pKa_1 = -1.0$$

$$\equiv SiOH \rightarrow \equiv SiO^- + H^+ \qquad pKa_2 = 4.0$$

The $SiOH$ surface groups are the predominant species. The surface concentration of $SiOH_2^+$ is highest at pH 0, whereas the concentration of SiO^- increases with increasing pH. At pH 8 the maximum concentration of SiO^- is found. (Duval Y., *et al* 2002) Therefore at environmentally relevant pH values (~5 to 8) the surface of silica is negatively charged. (Duval Y., *et al* 2002)

Atrazine [6-chloro-N^2-ethyl-N^4-isopropyl-1,3,5-triazine-2,4-diamine], one of the most common members of the *s*-triazine herbicide family, is one of the most widely applied herbicides in the world. In 1991 the United States Environmental Protection Agency (EPA) reported a steady use of herbicides from 1980 to 1990 of 500 million kg

of active ingredient per year in the USA. Approximately 363 million kg of atrazine were used between 1980 and 1990 in the USA. (Ralebitso T.K., *et al* 2002) Currently, atrazine is one of the two most commonly used herbicides in the United States. Between 29 and 34 million kg were applied in 2003 alone (EPA, 2003). Atrazine has been used since 1958 as a pre- and post-emergent herbicide to control broad leaf weeds in the production of corn, sweet corn (fresh and processed), sugarcane, sorghum, winter wheat, guava, nuts, hay, pasture, summer fallow, conifers, woody ornamentals, and Christmas trees among others. Atrazine is generally applied at rates of 1.12 to 2.24 kg/ha, which results in soil concentrations of 3 to 6 mg/kg. (Alvey S., and Crowley D., 1996)

The half life of atrazine varies greatly from 45 days (Protzman R., *et al* 1999) to 3-5 years (Armstrong D., *et al* 1967) depending upon the environmental conditions. The solubility of atrazine in water is 33 mg L^{-1} at 25 °C and it is fairly resistant to hydrolysis at neutral pH. In strong acids or alkaline solutions and temperatures greater than 70 °C atrazine hydrolyses to hydroxyatrazine and loses its herbicidal properties. (Worthing J. and Walker H., 1997) Atrazine can also be degraded at pH 6-8 by UV radiation with wavelengths less than 300 nm (maximum absorption occurs at 221 nm). (Comber S., 1999, Erickson E., *et al* 1989) Indirect and direct photolysis have been reported as degradation pathways. (Golberg M C., et al 1991)

As a consequence of atrazine widespread use and moderate persistence in the environment, it is frequently detected in ground and surface waters, in precipitation, and in gas phase. (Pereira W., *et al* 1990, Lode O., *et al* 1995, Bass. J. and Duyzer J., 1997,

Verstraeten P., *et al* 1999, Miller J., *et al* 2000) Detected concentrations in surface waters and groundwater are typically 100 ng L^{-1} or less although levels over 30 μg L^{-1} have been detected. (Cerejeira M., *et al* 2001, Garmouma M., *et al* 2001, Ren J., *et al* 2001)

The possible carcinogenic effect of *s*-triazine herbicides have been a subject of study since the late 80's. In 2002, several countries in Europe banned their use. Although the EPA classified atrazine as a "not likely human carcinogen" in 2003 it is still a suspected endocrine disrupting chemical in mammals and aquatic life. (EPA 2003, Islam M., *et al* 2002, Le Pennec G. and Le Pennec M., 2001, Moore A. and Lower N., 2001)

The European Union has proposed pesticide limits in drinking water of 0.1 μg L^{-1} (0.1 ppb) for an individual pesticide and a total concentration of pesticides and their degradation products to 0.5 μg L^{-1} (0.5 ppb). In the United States, the EPA has established a maximum contaminant level (MCL) for atrazine in drinking water of 3.0 μg L^{-1} (3.0 ppb).

Several investigations have been carried out on the adsorption of atrazine to clays. (Laird D., *et al* 1992, Konstantinou I., *et al* 2000, Clausen L., *et al* 2001, Herwig U., *et al* 2001, Lesan H., *et al* 2003) Despite the extensive work available on atrazine adsorption, and desorption processes, little is known at the molecular level about the interactions of atrazine with clays. Weakly basic herbicides such as the *s*-triazine herbicides can be adsorbed on clay minerals as both protonated and neutral species depending on the pH of

the solution. (Weber J., 1970) At pH values near to their pKa value, these weak base molecules are adsorbed as protonated species. Atrazine, with a pKa_1 of 1.60 and pKa_2 of 1.95, (Colombini M., *et al* 1998) is found as an uncharged molecule in the environment (pH ≈ 5 to 8). The neutral form of this weakly polar herbicide is adsorbed sparingly on clay mineral surfaces by weak physical forces. Atrazine may adsorb to clay surfaces by van der Waals forces or hydrogen bonding through its nitrogen atoms. (Weber J., 1970)

Sorption and exchange isotherm studies have suggested that protonated species of weak bases are adsorbed preferentially over neutral species even when the pH of the clay suspension is substantially greater than the equilibrium constant (pKa) of the molecule. (Ainsworth C., *et al* 1987) This phenomenon was attributed to surface acidity. (Calvet R., 1989) However, other sorption isotherm studies have shown that atrazine is primarily adsorbed on siloxane surfaces as a neutral species. These studies also suggest that neutral atrazine molecules are competitive with water molecules for solvation of low charge density siloxane surfaces but not for high charge density siloxane surfaces at neutral pH. (Laird D., *et al* 1994, Celis R., *et al* 1997) As a neutral molecule atrazine is weakly hydrogen bonded to siloxane surfaces and therefore is easily desorbed. (Barriuso E., *et al* 1994)

The results discussed above provide useful information about the sorption process of atrazine on clay minerals; however, the identity and orientation of the atrazine species at the surface of these clay minerals may have a large impact on the binding mechanism

of atrazine to clay minerals. In this study, a surface-selective technique, sum frequency generation (SFG) spectroscopy, is used to examine the air-solid interface of atrazine on silica, providing detailed molecular information about the distribution of this herbicide at the silica surface. This study provides the molecular level details required to evaluate the theories postulated from the macroscopic experimental results.

Since the present work focuses on the study of binding and adsorption properties of atrazine on the silica surface by SFG spectroscopy, a brief overview of SFG theory is presented. A more in depth discussion of the theory of sum frequency generation can be found in the literature. (Hirose C., *et al* 1992, Miranda P. and Shen Y., 1999, Shen Y. 1984)

SFG is a spectroscopic technique that has been extensively used during the past decade to study interfacial phenomena. SFG is a powerful technique for the elucidation of orientational and conformational information about interfacial species.

SFG is a second-order nonlinear process in which two pulsed laser beams, one with infrared frequency, ω_{IR}, and one with visible frequency, ω_{vis}, are overlapped in a medium in time and space, generating a photon at the sum of the frequencies, $\omega_{SFG} = \omega_{IR} + \omega_{Vis}$ is observed. Under the electric dipole approximation, the SFG process only occurs in noncentrosymmetric environments, such as an interface. The SFG intensity, I_{SFG}, is shown in Equation 1

$$I^{\omega_{SFG}}(\omega) \propto \left| E^{\omega_{SFG}} \cdot \chi^{(2)} : E^{\omega_{IR}} E^{\omega_{vis}} \right|^2 I^{\omega_{vis}} I^{\omega_{IR}} \tag{1}$$

where $I^{\omega_{SFG}}(\omega)$ is the intensity of the SFG and is a function of the frequency ω, $I^{\omega_{vis}} I^{\omega_{IR}}$ is the intensity of the incident visible multiplied by the incident infrared, and $\left| E^{\omega_{SFG}} \cdot \chi^{(2)} : E^{\omega_{IR}} E^{\omega_{vis}} \right|^2$ is the absolute square of the *E* field at the interface denoted by superscripts that define the frequency of the exigent (SFG) and the incident (visible and infrared) frequencies. *E* includes the Fresnel terms. The macroscopic second-order nonlinear susceptibility, $\chi^{(2)}$, is the tensor that describes the macroscopic susceptibility of the system and can be described as shown in Equation 2.

$$\left| \chi^{(2)} \right|^2 = \left| \chi_{NR}^{(2)} + \sum_{\nu} \chi_{\nu}^{(2)} \right|^2 \tag{2}$$

The macroscopic second-order nonlinear susceptibility, $\chi^{(2)}$, consists of a nonresonant term, $\chi_{NR}{}^{(2)}$, and resonant terms, $\chi_{\nu}{}^{(2)}$. When the frequency of the incident infrared beam, ω_{IR}, is resonant with a vibrational mode, ν, of an interfacial molecule the resonant susceptibility term, $\chi_{\nu}{}^{(2)}$, dominates and an SFG intensity enhancement is observed (the nonresonant term $\chi_{NR}{}^{(2)}$ is negligible for many surfaces).

Different polarization combinations of the incident and outgoing fields provide information about the molecular orientation at the interface. Liquid surfaces and interfaces are isotropic in the plane of the surface, and thus, symmetry constraints can reduce the surface susceptibility, $\chi_s^{(2)}$, from a 27-element tensor, to four independent

nonzero elements: $\chi^{(2)}_{zxx} = \chi^{(2)}_{zyy}; \chi^{(2)}_{xzx} = \chi^{(2)}_{yzy}; \chi^{(2)}_{xxz} = \chi^{(2)}_{yyz}; \chi^{(2)}_{zzz}$ where z is the direction normal to the interface. These four different elements contribute to the SFG signal under the four different polarization conditions PSS, SPS, SSP, and PPP. The polarizations are listed in the order of decreasing frequency: SF, *vis*, infrared. P-polarized light is defined as having its electric field vector parallel to the plane of incidence and S-polarized light has its electric field vector perpendicular to the plane of incidence. Spectra acquired with different polarization combinations can be compared to determine molecular orientation. (Zhang D., *et al* 1994)

When describing the sum frequency response, the linear and nonlinear Fresnel factors must also be taken into consideration. These factors relate the electric fields in the medium to the incident and exiting fields and describe the extent of transmission and reflection of the beams at the interface by considering the frequency, polarization, and the incident angle of the electromagnetic waves, and the indices of refraction for the media at the boundary. The intensity of the sum frequency emitted from the surface can be expressed in terms of the Fresnel coefficients as shown in Equations 3 to 6. (Zhuang P. *et al* 1999)

$$I_{ssp} \propto L_{yy}(\omega_{SFG}) L_{yy}(\omega_{vis}) L_{zz}(\omega_{IR}) \sin\theta_2 \chi_{yyz} \tag{3}$$

$$I_{sps} \propto L_{yy}(\omega_{SFG}) L_{zz}(\omega_{vis}) L_{yy}(\omega_{IR}) \sin\theta_1 \chi_{yzy} \tag{4}$$

$$I_{pss} \propto L_{zz}(\omega_{SFG}) L_{yy}(\omega_{vis}) L_{yy}(\omega_{IR}) \sin\theta \chi_{zyy} \tag{5}$$

$$
\begin{aligned}
I_{ppp} \propto & - L_{xx}(\omega_{SFG}) L_{xx}(\omega_{vis}) L_{zz}(\omega_{IR}) \cos\theta \cos\theta_1 \sin\theta_2 \chi_{xxz} \\
& - L_{xx}(\omega_{SFG}) L_{zz}(\omega_{vis}) L_{xx}(\omega_{IR}) \cos\theta \sin\theta_1 \cos\theta_2 \chi_{xzx} \\
& + L_{zz}(\omega_{SFG}) L_{xx}(\omega_{vis}) L_{xx}(\omega_{IR}) \sin\theta \cos\theta_1 \cos\theta_2 \chi_{zxx} \\
& + L_{zz}(\omega_{SFG}) L_{zz}(\omega_{vis}) L_{zz}(\omega_{IR}) \sin\theta \sin\theta_1 \sin\theta_2 \chi_{zzz}
\end{aligned}
\tag{6}
$$

where θ_i are the incidence angles (respect to the normal) of the optical field *E*, and L_{ii} (*i = x, y, z)* is the Fresnel coefficient determined by the refractive index of the two bulk phases and the interface layer, and the incident and reflected angles.

The resonant susceptibility term is proportional to the strength of the transition moment, A_ν, as shown in Equation 7

$$
\chi_\nu^{(2)} \propto \frac{A_\nu}{\omega_\nu - \omega_{IR} - i\Gamma_\nu} \tag{7}
$$

where A_ν is the amplitude of the transition moment, ω_ν is the frequency of the transition moment, and Γ_ν describes the line-width (half-width at half maximum) of the transition. The sign of A_ν indicates whether a transition is 90º out of phase with respect to the other transitions or if two transition moments exist anti-parallel with respect to each other; the resultant SFG response for both cases will then be 180º out of phase. The amplitude, A_ν, is nonzero when the Raman and the infrared transitions are spectroscopically allowed, meaning SFG is observed when the vibrational transitions are both Raman and infrared active. The macroscopic nonlinear susceptibility, $\chi^{(2)}$, is related to the molecular susceptibility, $\beta_{lmn,\nu}$. The molecular susceptibility can be described by equation 8

$$\beta_{lmn,v} = \frac{\langle g|\alpha_{lm}|v\rangle\langle v|\mu_n|g\rangle}{\omega_{IR} - \omega_v + i\Gamma_v} \tag{8}$$

where $\langle g|\alpha_{lm}|v\rangle$ represents the Raman tensor, $\langle v|\mu_n|g\rangle$ represents the infrared transition moment for the molecule, and *lmn* represents the molecular coordination system. An Euler angle transformation relates the molecular coordinate system (*l, m, n*) to the laboratory coordinate system *(I, J, K)*. The transformation is shown in equation 9

$$\beta_{IJK,v} = \sum_{lmn} \mu_{IJK:lmn}\beta_{lmn,v} \tag{9}$$

where $\mu_{IJK:lmn}$ is the Euler angle transformation between the laboratory coordinates (*I, J, K*) and the molecule coordinates (*l, m, n*). The macroscopic susceptibility, $\chi^{(2)}_{IJK,v}$, is therefore calculated from the molecular susceptibility, $\beta_{IJK,v}$, as shown in equation 10

$$\chi^{(2)}_{IJK,v} = N\langle\beta_{IJK,v}\rangle \tag{10}$$

where $\chi^{(2)}_{IJK,v}$ is equal to the number density , *N*, multiplied by the orientation average of $\beta_{IJK,v}$.

The objective of this thesis work is to determine the binding mechanisms of atrazine adsorption on the silica surface to better understand it mobility in the environment.

CHAPTER 2

EXPERIMENTAL

2.1 Instrumentation

2.1.1 Raman Instrumentation

Raman spectra were obtained using a 785 nm continuous wave laser (Process Instruments) with an energy 225 mW. The backscattered light was collected by a fiber optic probe (InPhotonics) coupled to the entrance slit of 500-mm monochromator (Acton Research SpectraPro SP-500) using a 1200 groove/mm grating blazed at 1μm. The slit width was set to 100 μm, and the band pass varied between 2.142 cm^{-1} (at 400 cm^{-1}) and 1.503 cm^{-1} (at 3300 cm^{-1}). The Raman spectra were collected in 6 min exposures to a liquid nitrogen cooled CCD camera (Roper Scientific LN400EB, 1340 x 400 pixel array, back-illuminated and deep depletion). CCD calibration was completed by using the 435.83 nm line from a fluorescent lamp. The calibration of the wavenumber position was completed by taking a spectrum of crystalline naphthalene and comparing peak positions with the literature values. (McCreery R. L., 2000)

2.1.2 Fourier Transformation Infrared (FTIR) Instrumentation

Experiments were performed in a Thermo Nicolet FTIR spectrometer (Avatar 370, Thermo Electron Corporation). Transmission mode was employed by using the KBr pellet technique for atrazine and its degradation products. The spectral resolution was 4 cm^{-1}. The spectra were averaged over 64 scans.

2.1.3 SFG Instrumentation

SFG scanning experiments were carried out using a visible beam at 532 nm and infrared beam tunable from 2500 to 4000 cm^{-1} with a bandwidth of ~8 cm^{-1} generated from a KTP-KTA based optical parametric generator/amplifier (OPG/OPA) system (Laser vision), Figure 2.1. The 532 nm beam was generated by doubling the frequency (second harmonic) of the 1064 nm pump source from a EKSPLA PL 2143 A/SS Nd: YAG laser (29 ps pulse duration and 10 HZ repetition rate). A color glass filter (BG25, 2 mm thickness, CVI Laser) followed by a short pass filter (SPF500, CVI Laser) and two holographic notch plus filters (Kaiser Optical System, Inc) in the detection system are used for filtering out the scattered 532 nm light. A 512 x 512 pixel array, 16 μm^2 square pixel size, back illuminated charge-couple device (CCD) (DV8, Andor Technology) was used to detect the sum frequency signal. The CCD was thermoelectrically cooled, and the temperature was set at ~ -80 °C during the experiments.

The scanning SFG system control software was programmed in the Allen laboratory using Labview and C+ programming languages. The program integrates automation control of the OPG/OPA servomotor, an infrared energy meter control, (EPM 2000, Molectron Inc.), and CCD image acquisition and data analysis. At least one air-neat water spectrum was acquired at the beginning and end of the experiment to ensure the stability of the SFG system and to confirm reproducibility. A real-time background subtraction algorithm was applied, and the spectra showed that the background baseline intensity did not add to the overall intensity of the SFG spectra.

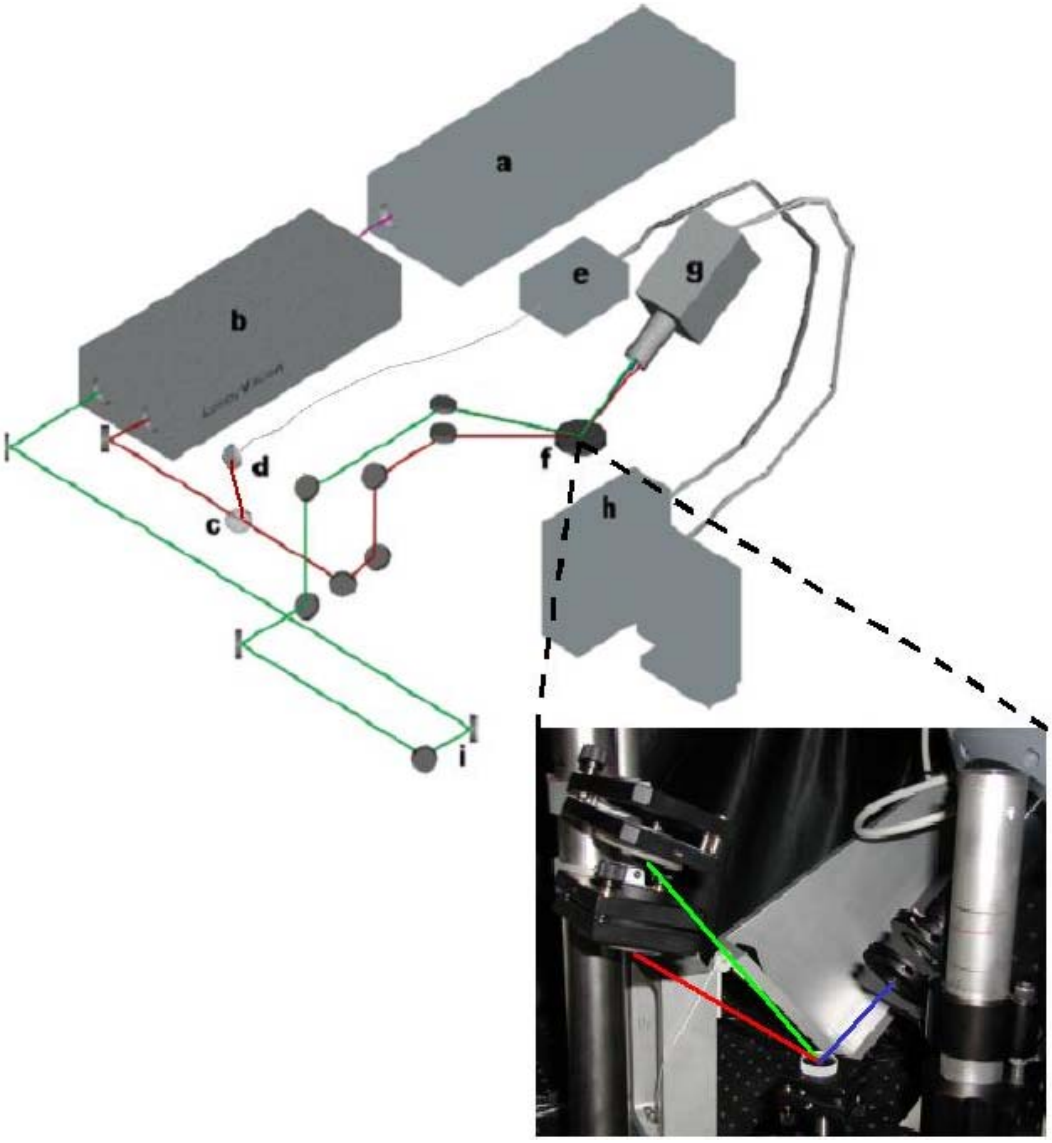

Figure 2.1. Schematic layout of the vibrational sum frequency generation scanning system: (a) Nd:YAG laser; (b) LaserVision OPA/OPG; (c)infrared window; (d) infrared detector; (e) energy meter; (f) sample stage; (g) CCD; (h) control computer; (i) delay line. Green, red, blue, and pink solid lines represent 532 nm, infrared, sum frequency, and 1064 nm, respectively. Picture shows the sample stage and the paths of the incoming and outcoming beams.

The SFG was initially optimized spatially and temporally at 3300 cm^{-1} since this is the center of the scanning region (2900-3900 cm^{-1}). The SFG spectra were normalized by the IR profile, which was detected in real-time with the SFG intensity. The polarization combinations used for the SFG experiments were S, S, and P for the SFG, 532 nm, and infrared beams respectively. Additional spectra with $S_{SFG},P_{vis}S_{IR}$, $P_{SFG},P_{vis}P_{IR}$, and $P_{SFG},S_{vis}S_{IR}$ polarization were acquired for the assignment of the CH vibrational modes. All of the SSP-polarized spectra were acquired using a 10 s exposure time for each data point and were acquired in ~30 min (from 2800 to 3900 cm^{-1}). All the SFG spectra were acquired at ~23 ° C and in a range from 30 to 45% RH.

2.2 Sample Preparation

Atrazine (98%), atrazine-desethyl (97%) [6-chloro-N^4-isopropyl-1,3,5-triazine,4-amine], (ADE), and atrazine-desisopropyl (97%) [6-chloro-N^2-ethyl-1,3,5-triazine-2-amine], (ADI), were obtained from Riedel-de Haën, Germany, methanol (>99.9 purity), and chloroform (HPLC grade) were supplied by Sigma-Aldrich (PA, USA). All the chemicals were used as received. Infrared grade fused silica plates of 1.00 inch diameter and 0.188 inch thickness were obtained from Quartz Plus Inc.

All glassware used was cleaned with an ammonium peroxydisulfate in sulfuric acid solution (0.08 M) to eliminate trace organics and rinsed with nano-pure water from a Millipore Nanopure system (18.3 MΩ·cm).

Infrared grade fused silica plates were annealed in a muffle oven (Fisher Scientific, Isotemp Muffle Furnace) at 900 °C for 12 hours to eliminate any chemically and physically adsorbed organic substances. The silica plates were then cooled to room temperature, and allowed to reach equilibrium with the water vapor from air for 30 min.

Water, pure chloroform, pure methanol, and solutions of atrazine in chloroform were added to different silica plates. Silica plates were placed at ~ 45 º of inclination, then ~ 300 μL of the solutions were slowly added to cover the surface of the silica plate. The silica plates were allowed to dry at room temperature. Scanning SFG spectroscopy was used to analyze the adsorption of each chemical species at the air-silica interface as well as the silica surface before exposure to any chemical solution.

2.3 *Ab Initio* Calculations

Calculations were preformed using Gaussian 03 for Windows at the HF level of theory with a 6-31+G* basis set was chosen for all *ab initio* calculations (Frisch M. *et al* 2003)

2.4 Spectral Fits

All spectral fits shown in this paper were performed using the software package IGOR (version 4.0.5.1). A Lorentzian fitting function written to incorporate phase was invoked by IGOR to fit the spectra. The SFG spectrum, which is a plot of the SFG intensity (I_{SFG}) as a function of the incident infrared frequency, ω_{IR}, can be mathematically fit according to Equations (1) and (7). When performing the fit, a

constant complex number is used as the non-resonant term $\chi_{NR}^{(2)}$ and the sign of the amplitude (A_v) is used to denote the phase of the photons of the vibrational mode from the interfacial molecules, which incorporates orientation and relative vibrational phases. Equations (7) and (2) indicate the Lorentzian line shape in the SFG spectrum fitting. The SFG the intensity is proportional to the absolute square of the summation of each vibration's $\chi_v^{(2)}$ and $\chi_{NR}^{(2)}$ as shown in Equation (2). Therefore, SFG spectral interpretation must occur after deconvolution into the component peaks since direct comparison of SFG spectra to Raman and IR spectra may be misleading, in particular for the broad bands of the hydrogen bonding region (3000 – 3600 cm^{-1}).

CHAPTER 3

RESULTS AND DISCUSSION

The air – solid interface of atrazine adsorbed on silica was investigated because the orientation of molecules at an interface ultimately determines the availability of reactive functional groups to interact with their surroundings. Thus, in this model system the interaction of atrazine and silica and the effect of water deposited on the silica surface after atrazine adsorption were analyzed.

The molecular structures of atrazine, and its dealkylated degradation products, atrazine-desethyl (ADE), and atrazine-desisopropyl (ADI) are shown in Figure 3.1.

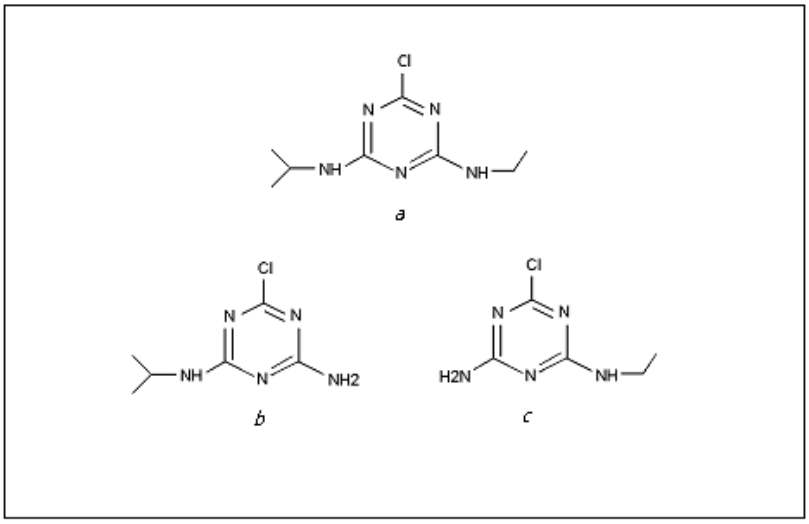

Figure 3.1 Molecular structures of (a) atrazine, (b) ADE, and (c) ADI.

3.1. Air-silica interface after exposure to solvents

A solution containing atrazine was introduced to the silica surface. This required a solvent that would not interact with the silica surface so as to only observe the interaction of atrazine with the silica surface. Atrazine is soluble in water (33 mg L^{-1} at 25 °C), methanol (18 g L^{-1} at 25 °C), and chloroform (52 g L^{-1} at 25 °C). (Windholz M., 1976) These three solvents were used (see experimental section 2.3 for exposure details). Silica surfaces were first analyzed after the addition of water, neat methanol, and neat chloroform. The SFG spectra of the air-silica interface after the addition of each solvent were obtained using the SSP polarization combination and are shown in Figure 3.2 a-c. The spectrum of the air – silica surface before exposure to any solvent is also shown for comparison.

The spectrum of the clean air - silica interface (Fig. 3.2 a-c) obtained at 35% RH shows a weak and broad feature from 3100 cm^{-1} to 3600 cm^{-1} that is assigned to hydrogen bonded OH stretching bands, and a strong free silanol OH stretching peak at ~ 3750 cm^{-1} (≡SiOH) (Parks G., 1984). Upon addition of water to the silica surface the spectrum (Fig. 3.2, a) reveals a decrease in the intensity of the free silanol OH stretch peak, suggesting that water interacts with the OH groups on the silica surface, through hydrogen bonding. This result is in agreement with previous studies of the silica surface. (Du Q., *et al*, 1994, Iler R., 1979, Duval Y., *et al* 2002) Additionally, an enhancement in the 3400 cm^{-1} region is observed and is assigned to hydrogen bonded OH stretching modes.

The SFG spectrum after addition of methanol to the silica surface shows a decrease in the intensity of the free silanol OH peak (Fig. 3.2 b). An increase in the intensity in the 3000 cm^{-1} - 3600 cm^{-1} region is also observed and assigned to hydrogen bonded OH stretching modes. An interesting feature is that no peak is observed in the CH stretching region (~ 2900 cm^{-1}). From these results two possible scenarios can be proposed: 1) methanol interacts with the surface silanol OH groups at the silica surface, likely through hydrogen bonding, however the amount of adsorbed methanol is below the detection limit and no CH stretch peak is observed, and 2) trace amounts of water in the methanol added to the silica surface are adsorbed (methanol molecules evaporate before interacting with the silica surface).

In order to determine if the methanol molecules or water molecules were adsorbed, a second spectrum was obtained of the same silica plate after 12 hr of exposure

to ambient conditions (~30% RH), (Fig. 3.3). The spectrum of clean silica is shown for comparison. There is no change in the intensity of the free silanol OH stretch peak at ~ 3750 cm^{-1} in the spectra acquired before and after 12 hr of exposure to ambient conditions. In the spectrum obtained after 12 hr of exposure to air, an enhancement in the 3400 cm^{-1} region relative to that of the spectrum acquired before exposure (Fig. 3.2 b) is observed. This enhancement is attributed to adsorption of water molecules from the air to the silica surface. The water molecules are adsorbed to the previously adsorbed molecules (methanol or water) at the silica surface and not to the silanol OH groups at the silica surface, since no further decrease in intensity of the free silanol OH peak was observed.

Based on the results discussed above, the decrease in the intensity of the free silanol OH peak in the SFG spectrum after methanol exposure can be attributed to the two possible reasons, methanol or water molecules adsorbed. An analysis of the silica surface after methanol exposure at 0% RH is suggested to elucidate with molecule (water or methanol) is responsible for the decrease in the intensity of the free silanol OH peak.

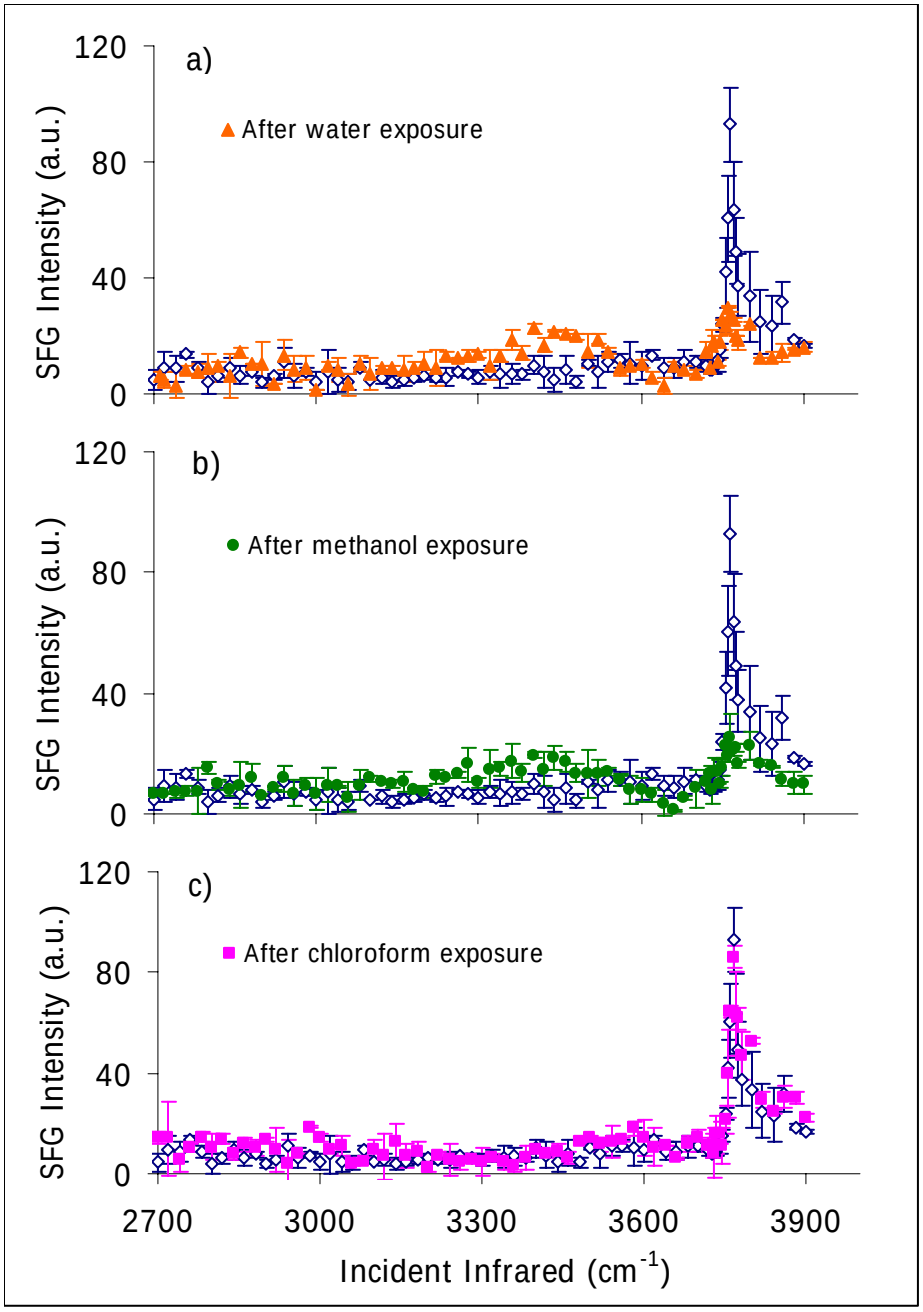

Figure 3.2. SSP-polarized SFG spectra of the silica surface after exposure to a) water, b) neat methanol, and c) neat chloroform. The spectrum of the air – silica interface before exposure is shown in open diamonds.

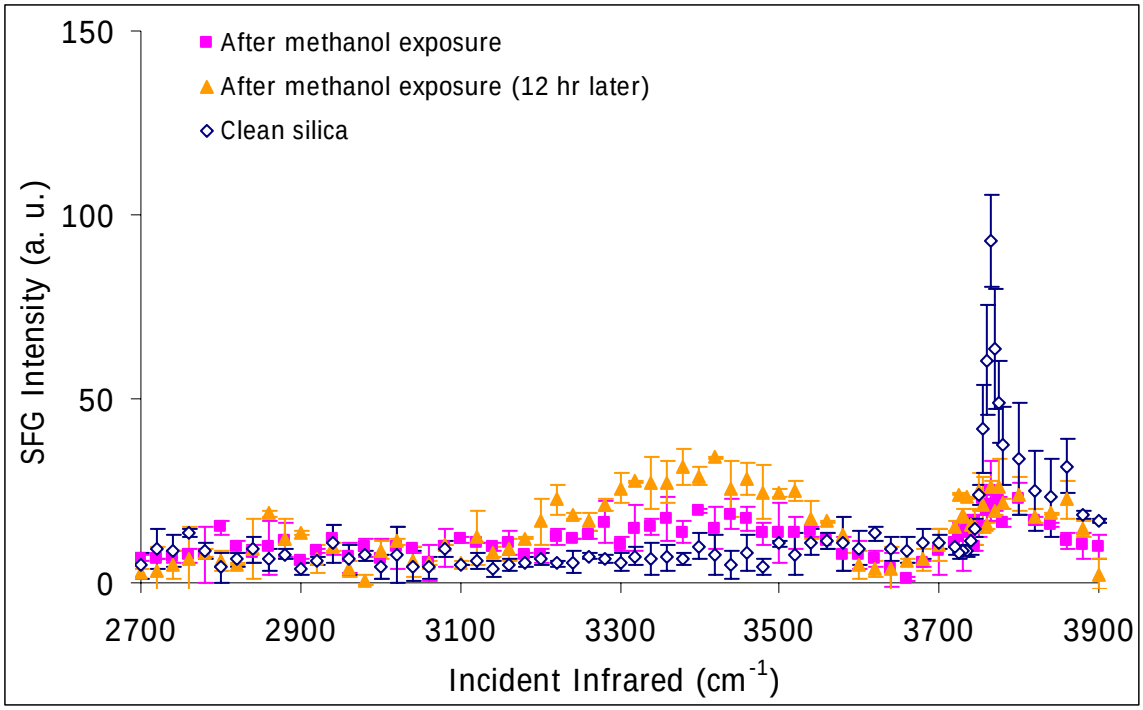

Figure 3.3. SSP-polarized SFG spectra of the silica surface after methanol exposure before and after 12 hr of exposure to atmospheric conditions. The clean silica surface is shown for comparison.

After addition of chloroform to the silica surface the SFG spectrum presents the same features as the clean silica spectrum (at 35% RH), Fig. 3.2, c. The broad peak from 3100 cm^{-1} to 3600 cm^{-1}, and the peak corresponding to free silanol OH stretch at 3750 cm^{-1} are identical to those found on the clean surface within experimental error. This suggests that chloroform does not interact with the surface silanol OH groups nor water carried in via the chloroform liquid. Additionally, no peaks were observed in the CH region (~ 2900 cm^{-1}). This also suggests that chloroform does not interact with the silica surface.

Hydrogen bond acidity is defined as the ability to donate the hydrogen atom to form a hydrogen bond. (Abraham M., *et al* 1989) A scale of hydrogen bond acidity based on equilibrium constants (as *log* K_a) assigned values to water, methanol, and chloroform of 0.353, 0.367, and 0.197 respectively. (Abraham M., *et al* 1989). These values indicate that methanol and water are similar in their abilities to donate the hydrogen atom to form a hydrogen bond, whereas chloroform is less effective in donating the hydrogen atoms to form hydrogen bonds, as one would expect. After the analysis of the spectra shown in Figure 3.2 a-c, chloroform was chosen as the best solvent for the introduction of atrazine as it does not interact with the surface silanol groups.

3.2.Air-silica interface after exposure to atrazine in chloroform solutions

Atrazine solutions from 0.01 mM to 0.55 mM prepared in chloroform were added to the silica surface and allowed to evaporate. The addition was completed by spreading 300 μL of atrazine in chloroform solution over the silica plate surface. The SSP-polarized SFG spectra of the air - silica interface after exposure to the atrazine in chloroform solutions were obtained and are shown in Figure 3.4 a-c. The insets show an expanded view of the free silanol region (Fig. 3.4 b) and NH region (3100 - 3600 cm^{-1}) (Fig. 3.2 c) of the spectra. The clean silica surface spectrum is shown for comparison.

The SFG spectrum of the air – silica interface after exposure to a 0.1 mM atrazine in chloroform solution reveals a decrease in the intensity of the free silanol OH peak, accompanied by the appearance of small peaks in the CH stretching region (~ 2900 cm^{-1}),

as shown in Fig. 3.4 a. With increasing atrazine concentration, the intensity of the free silanol OH peak decreases, while the intensity of the CH stretching peaks (~ 2900 cm^{-1}) increases, Fig. 3.4 a. The free silanol OH peak is not observed in the SFG spectrum of the air – silica interface after exposure to a 0.55 mM atrazine chloroform solution, Fig. 3.4 b. Also in this spectrum two prominent peaks at ~ 2880 cm^{-1} and ~ 2960 cm^{-1}, and a relatively small peak at ~ 2920 $cm^{-1}$is observed, as shown in Fig. 3.4 a. Additionally, a broad peak ~ 3250 cm^{-1}, and a small peak at ~ 3440 cm^{-1} are observed, Fig. 3.4 c. The peaks observed in the CH stretching region (~ 2900 cm^{-1}) are due to atrazine molecules and not to chloroform (the CH stretch peak from chloroform was not detected in previous experiment, Fig. 3.2 c). To aid in making the spectral assignments of the SFG spectra in the CH and NH stretching region, the Raman and infrared spectra of powdered atrazine were acquired and are shown in Figure 3.5.

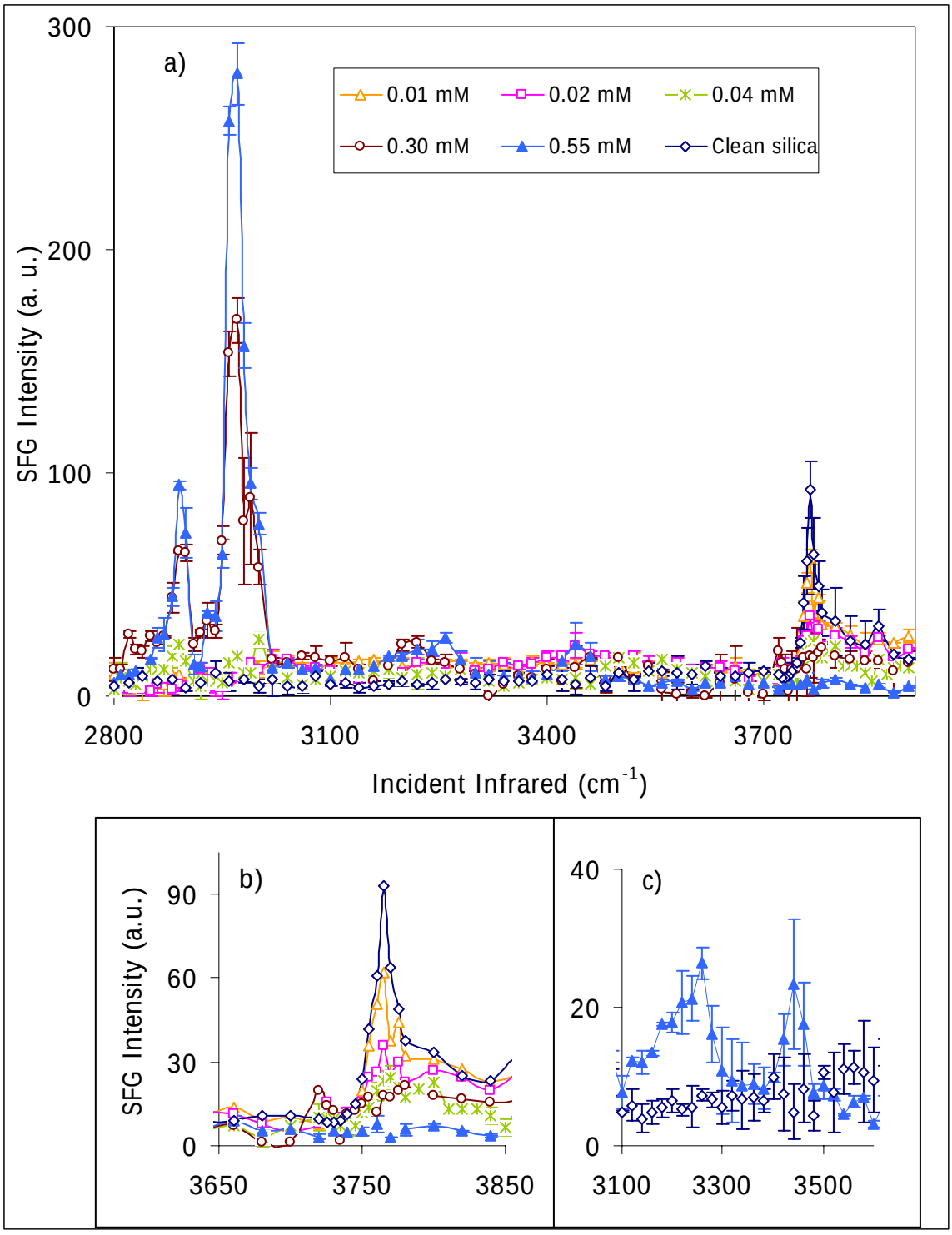

Figure 3.4 a) SSP-polarized SFG spectra of atrazine in chloroform solutions from 0.01mM to 0.55mM onto silica. The insets show an expanded view of b) the free silanol OH stretch region, and c) the NH region (3100 - 3600 cm^{-1}).

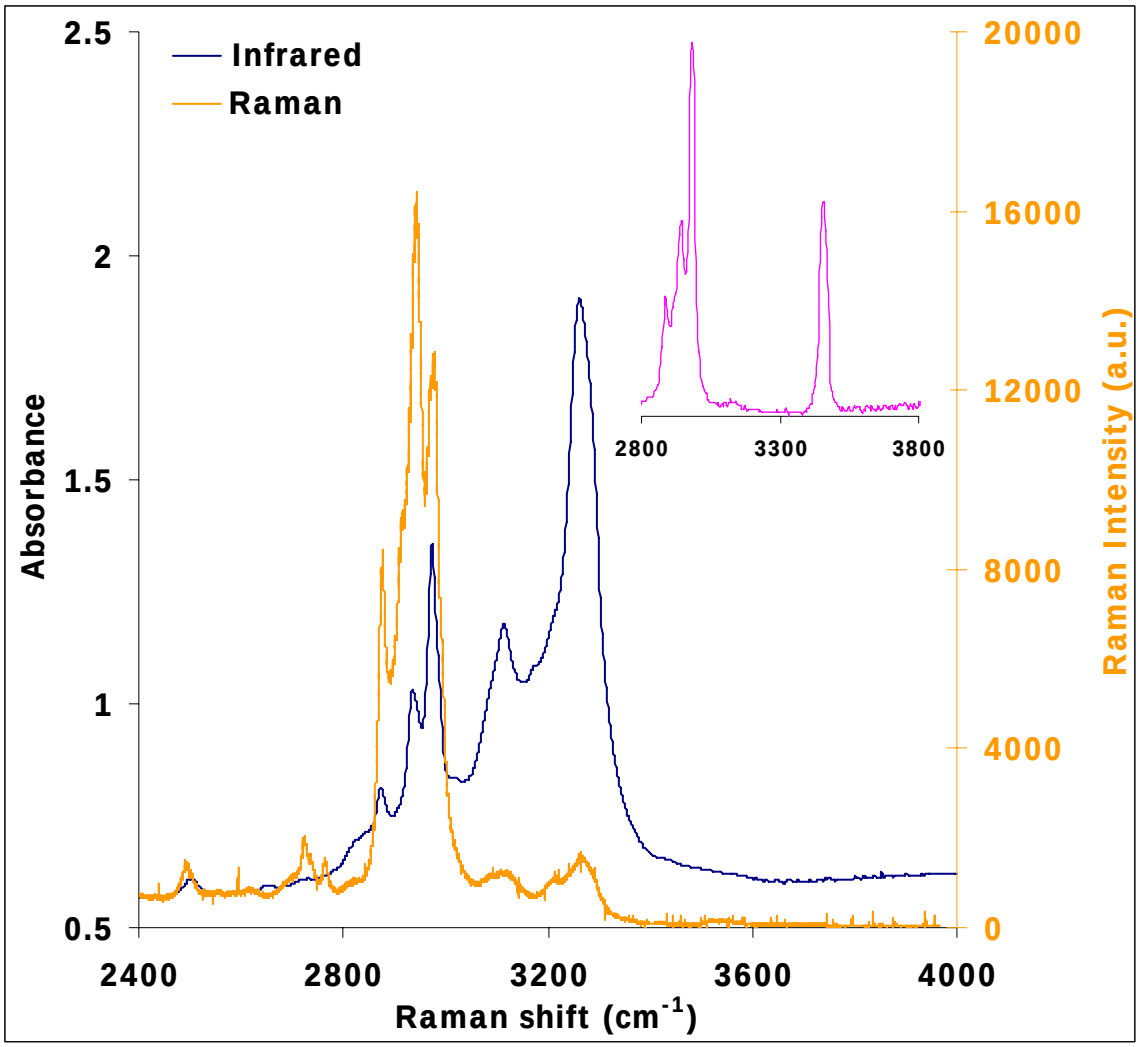

Figure 3.5 Infrared and Raman spectra of the solid phase of atrazine. The inset shows the infrared spectrum of atrazine in the gas phase reported by NIST (Standard Reference Data Program, Collection (C) 2003). All rights reserved.

3.2.1.Assignments of NH and CH vibrational modes

Atrazine has ethylamine and isopropylamine groups attached to the chlorinated *s*-triazine ring as in shown in Figure 3.1 a. The gas phase infrared spectrum of secondary amines shows only a single NH stretch at ~ 3460 cm^{-1} as shown in the inset of Figure 3.5. In infrared studies when self-association occurs in the solid phase, a second band at lower frequency is also observed. (Bellamy L., 1975) In both the Raman and infrared spectra two broad peaks at ~ 3115 cm^{-1}, and ~ 3260 cm^{-1} are present and are assigned to the NH stretch, Fig. 3.5. The lower frequency, ~ 3115 cm^{-1} peak is usually attributed to the bonded NH, and the higher frequency, ~ 3260 cm^{-1} peak to the free NH. (Bellamy L., 1975)

Higher intensities of the NH bands relative to the CH bands are observed in the infrared spectrum compared to those of the Raman spectrum, Fig 3.5. This difference in the NH peak intensity can be attributed to the different selection rules of infrared and Raman spectroscopy; for a mode to be infrared active the vibration must cause a change in dipole moment, whereas for a mode to be Raman active, there must be a change in polarizability. Thus, the NH vibrational modes of atrazine cause a more pronounced change in dipole moment than in polarizability.

SFG studies of the air-neat water interface have shown peaks at ~ 3250 cm^{-1}, and ~ 3450 cm^{-1} attributed to different OH stretches of the interfacial water molecules. (Du Q. *et al*., 1993, Schnnitzer C. *et al*., 1999, Allen H. C. *et al*., 2000, Allen H. C. *et al*., 2001). The SSP polarized SFG spectrum of a 0.55 mM atrazine in chloroform adsorbed on silica shows two peaks at ~ 3250 cm^{-1} and ~ 3440 cm^{-1} (Fig. 3.4 c) that cannot be attributed to water adsorbed on the silica surface since their intensity increases with increasing atrazine concentration, Fig. 3.4 a. Therefore, these peaks are attributed to NH stretch vibrational modes. A considerable shift in the frequencies of the NH vibrational mode from the Raman and infrared spectra of atrazine (~ 3115 and ~ 3260 cm^{-1}) and the SFG spectrum of atrazine adsorbed on silica (~ 3250 and ~ 3440 cm^{-1}) is observed. The assignment of the peak at ~ 3440 cm^{-1} is consistent with previous infrared studies of silica and amino groups. (William H., 1973)

In both Raman and infrared spectra the CH stretching region (2800-3000 cm^{-1}) consists of only partially resolved peaks, Fig. 3.5. Deconvolution of the CH stretching vibrational bands in the 2800-3000 cm^{-1} region is non-trivial; in addition to the fundamental vibrational modes involving symmetric and asymmetric stretching from the CH_2 and CH_3 groups, the Fermi resonances of bending mode overtones with fundamental modes are also present (Ru L., *et a*l 2004). Three peaks at ~ 2875 cm^{-1}, ~ 2940 cm^{-1}, and ~ 2975 cm^{-1} are observed in both Raman and infrared spectra and are assigned to CH stretch vibrational modes.

The degradation products of atrazine, ADE and ADI, contain a chlorinated *s*-triazine ring. ADE has only CH and CH_3 groups in the isopropylamine group attached to the ring, while ADI contains only CH_2 and CH_3 groups in the ethylamine group attached to the ring (Figure 3.1 b-c). To simplify the CH stretching region and thus, clarify the peak assignment, the infrared and Raman spectra of ADI and ADE solid phase (powder) were acquired and are shown in Figure 3.6 a-b. The Raman and infrared spectra of powdered atrazine are also shown for comparison.

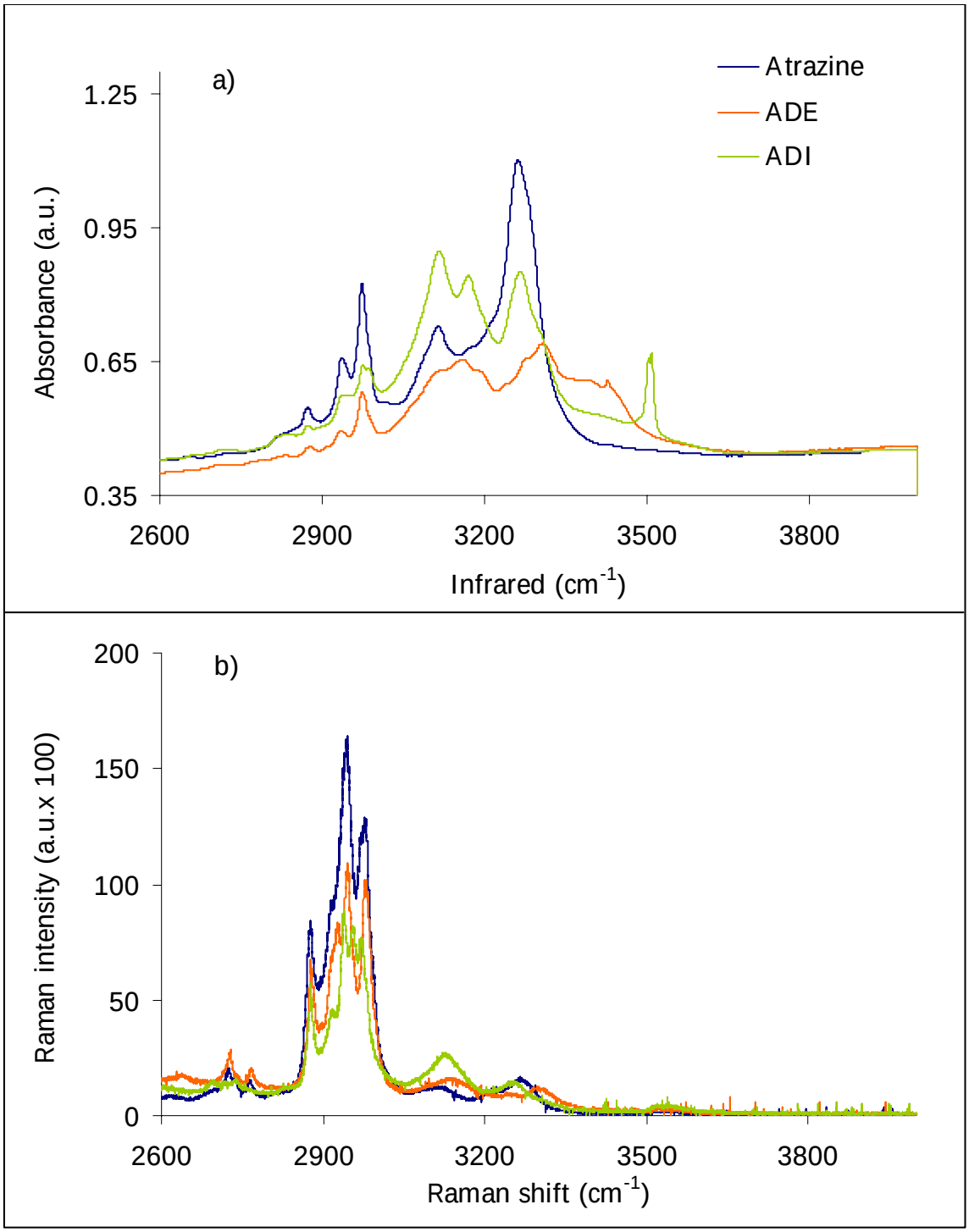

Figure 3.6. a) Infrared and b) Raman spectra of the solid phase of atrazine, ADE, and ADI.

The Raman and infrared spectra of all three compounds show a CH stretching region (2800-3000 cm^{-1}), consisting of partially resolved peaks. The ADE and ADI spectra show three main peaks at ~ 2875 cm^{-1}, ~ 2940 cm^{-1}, ~ 2975 cm^{-1} that are assigned to CH_3 vibrational modes. The peaks at ~ 2875 cm^{-1} are attributed to the CH_3 symmetric stretch mode ν_s. The peaks at ~ 2940 cm^{-1} are assigned to the Fermi resonance of the CH_3 ν_s stretching mode with the overtone of the CH_3 bending mode, and the peaks at ~ 2975 cm^{-1} are assigned to the CH_3 asymmetric stretch mode ν_{as}. These assignments are based on SFG studies of organic molecules reported by Guyot P., *et al* (1987), Lu R., *et al* (2004), Wang C., *et al* (2003), Murphy W., *et al* (1993).

Both the ADE and ADI infrared spectra show greater intensities in the NH bands relative to the CH bands compared with those of the Raman spectra, Fig. 3.6. This is attributed to different selection rules of infrared and Raman. The ADI infrared spectrum shows a narrow peak around 3500 cm^{-1} that is assigned to NH asymmetric stretch mode, Fig. 3.6 a. This band is not well resolved in the ADE infrared spectrum. In addition, the NH region (3200 – 3600 cm^{-1}) of the ADE and ADI infrared spectra shows peaks at ~ 3170 cm^{-1}, assigned to the NH vibrational modes product of intermolecular hydrogen bonding, Fig. 3.6 a. (Bellamy L., 1975) A summary of the peak assignments from Raman and infrared spectra of powdered atrazine, ADE, and ADI is listed in Table 3.1.

Frequencies (cm^{-1})	Assignment
~ 2875	CH_3 ν_s
~ 2940	Fermi Resonance CH_3
~ 2975	CH_3 ν_{as}
~ 3115	Bonded NH
~ 3260	Free NH

Table 3.1. Summary of the peak assignments from Raman and infrared spectra of powders of atrazine, ADE, and ADI.

From the Raman and infrared spectra results of atrazine, ADE, and ADI the peak at 2884 cm^{-1} of the SSP-polarized SFG spectrum of the air – silica interface after exposure to atrazine (Fig. 3.4 a) is attributed to the CH_3 ν_s. However, the Raman and infrared spectra resolution is limited by the chemical system (due to the number of CH vibrational modes of the atrazine and its degradation products) in the area from 2900 cm^{-1} to 3000 cm^{-1} is not sufficient to assign the two peaks at ~ 2919 cm^{-1}, and ~ 2966 cm^{-1} in the SFG spectrum (Fig. 3.4 a).

The calculated fit and component peaks of the SSP- polarized SFG spectrum of the air – silica interface after exposure to a 0.55 mM atrazine in chloroform of the CH stretching region (2800 cm^{-1} – 3100 cm^{-1}) were obtained and are shown in Figure 3.7.

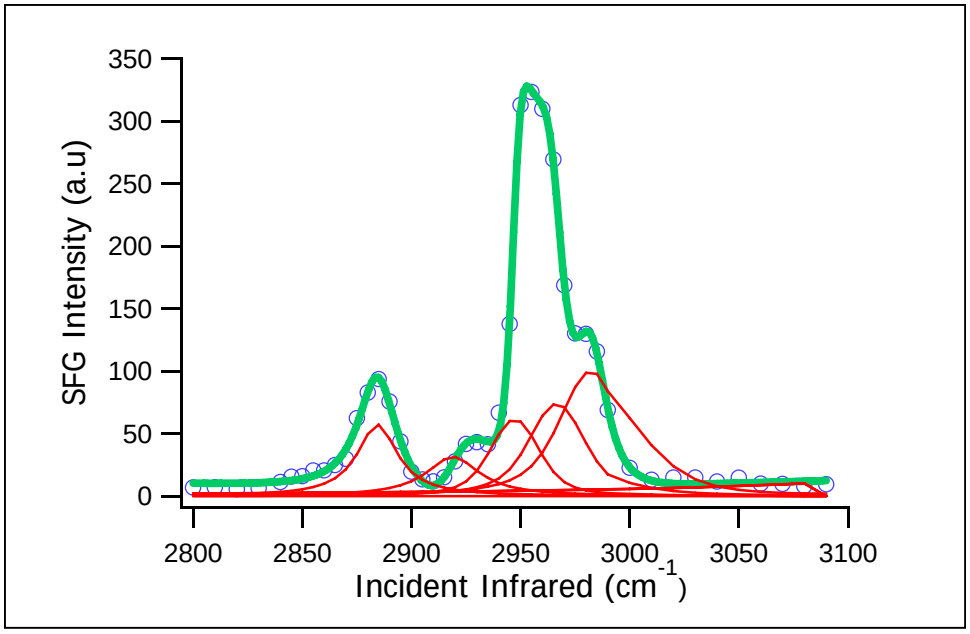

Figure 3.7. Spectral fit of the SSP-polarized SFG spectrum of 0.55 mM atrazine in chloroform onto the silica surface. The component peaks are shown in red, the calculated spectrum from the spectral fit is shown in green, which pass through the experimental data, and the data points are shown in blue circles.

Previous work has shown the sum frequency active modes in the CH stretching region under SSP polarization (Gragson D., *et al* 1996, Wang C., *et al* 2003, Lu R., *et al* 2004, Yang M., *et al* 2004) The deconvolution of the SSP – polarized spectrum (Figure 3.7.) shows component peaks at 2884 cm^{-1}, 2919 cm^{-1}, 2947 cm^{-1}, 2966 cm^{-1}, 2983 cm^{-1}, and 3316 cm^{-1}. The frequencies at 2966 cm^{-1}, and 2983 cm^{-1} are in the same phase with each other. All other are the in opposite phase with respect to them (- versus +) (see equation (7) description for details of phase). From the Raman and infrared spectra results previously discussed, the frequencies at 2884 cm^{-1}, 2947 $cm^{-1,}$ and 2983 cm^{-1} are

assigned to CH_3 ν_s, CH_3 Fermi resonance, and CH_3 ν_{as} respectively. The component peak centered at 2919 cm^{-1} in the SFG spectrum is not clearly observed in the infrared spectrum of the powdered atrazine, but a shoulder at ~ 2920 cm^{-1} in the Raman spectrum is observed (Fig. 3.5). This peak is attributed to the asymmetric stretch, CH_2 ν_{as}, based on SFG studies of surfactants reported by Messmer M. C., *et al* 1995. The peak at 2966 cm^{-1} in the SFG spectrum is attributed to a second component of CH_3 ν_{as} based on SFG and infrared studies of small organic molecules. (Wang C., *et al* 2003, Zeroka D., and Jensen J., 1998) The peak at 2983 cm^{-1} was also assigned to the CH_3 ν_{as} from the Raman and infrared results obtained in this thesis. The assignment of two frequencies to the same vibrational mode may arise due to two reasons; a) there are two types of CH_3 groups in atrazine, namely in the ethyl and isopropyl side chains, and b) these vibrations are degenerate if the point group symmetry of the CH_3 groups is C_{3v}. However the amine group may break this symmetry lifting the degeneracy.

It is well known that the CH frequencies are dependent upon the local environment, and in particular on the nature of atoms or groups which lie in the *gauche* position. (Bellamy L., 1980) Infrared and theoretical studies of amines have assigned the CH_3 asymmetric stretch ν_{as} to peaks at ~ 2965 cm^{-1}, and ~ 2986 cm^{-1} for isopropylamine and ethylamine respectively. Although under certain symmetry constraints *trans*-ethylamine also presents a band at 2961 cm^{-1}. From these studies it can be proposed that the band at 2966 cm^{-1} arises from the CH_3 ν_{as} of isopropylamine, and ethylamine, whereas the band at 2983 cm^{-1} comes from CH_3 ν_{as} of ethylamine. (Zeroka D., *et al* 1999 (I), Zeroka D., *et al* 1999 (II)).

Infrared studies of melamine derivatives where methyl groups were adjacent to an oxygen atom, two CH_3 asymmetric stretches were assigned to an in-phase stretch and out-of phase stretch for a single methyl group. (Larkin P J., *et al* 1998) Atrazine consists of a chlorinated *s*-triazine ring with two amines, isopropylamine and ethylamine attached to it (Figure 3.1 a). NMR, and theoretical studies have demonstrated that atrazine exists as a mixture of four conformational isomers related by rotation of the alkylamino side chains. The existence of these four conformers is the result of the delocalization of the nitrogen lone pair electrons into an adjacent π-electron system, generating resonance structures, Figure 3.8 a-b. (Almeida W., and Malley P., 1992, Welhouse G., and Bleam W., 1992) Infrared, Raman, and SFG studies of aromatic compounds such as toluene, and *m*-xylene have assigned two CH_3 asymmetric stretch vibrations to ~ 2950 cm^{-1} and ~ 2984 cm^{-1} bands. (Hommel E., and Allen H., 2003) It can be then proposed that the aromaticity and the presence of nitrogen atoms adjacent to the CH_3 groups in atrazine may disturb the point group symmetry C_{3v} lifting the degeneracy.

In order to determine spectral assignments in the CH stretching region *ab initio* calculations were performed using Gaussian 03 for Windows at the HF level of theory with a 6-31+G* basis set. Gopenmol, molecular modeling software, was used to visualize the vibrational modes. (Laakson L., 1992, Bergman D., *et al* 1997) A summary of the frequencies observed, their assignments, and the amine where the CH groups are located is listed in Table 3.2. These results show that CH_3 symmetric stretches ν_s arise from the CH_3 groups of ethylamine and isopropylamine within 2885 and 2891 cm^{-1}. The CH_3 asymmetric stretches clearly appear in two different regions 2940-2962 cm^{-1} and 2983-

2989 cm^{-1}. Ethylamine and isopropylamine present CH_3 asymmetric stretches in both regions. Therefore, the first possible reason of the assignment of the two CH_3 ν_{as} to the two types of CH_3 groups from the ethyl and isopropyl side chains is excluded. The second possibility is that the assignment of the two CH_3 ν_{as} is due to the aromaticity and the presence of nitrogen atoms that disturb the C_{3v} point group symmetry lifting the degeneracy. Based on these results, reason two is the potential explanation to the presence of two CH_3 ν_{as} in atrazine. Consequently, the peaks at 2966 cm^{-1} and 2983 cm^{-1} are attributed to the in phase CH_3 ν_{as}, and out-of phase CH_3 ν_{as}, respectively.

Frequencies (cm^{-1})	Assignment	Amine
2885	CH_3 ν_s	Ethylamine
2887	CH_3 ν_s	Isopropylamine
2891	CH_3 ν_s	Isopropylamine
2919	CH_2 ν_{as}	Ethylamine
2940	CH_3 ν_{as}	Isopropylamine
2944	CH_3 ν_{as}	Isopropylamine
2962	CH_3 ν_{as}	Ethylamine
2983	CH_3 ν_{as}	Isopropylamine
2988	CH_3 ν_{as}	Isopropylamine
2989	CH_3 ν_{as}	Ethylamine

Table 3.2. Summary of the frequencies obtained from *ab initio* calculations, their assignment, and the amine where the CH groups are located.

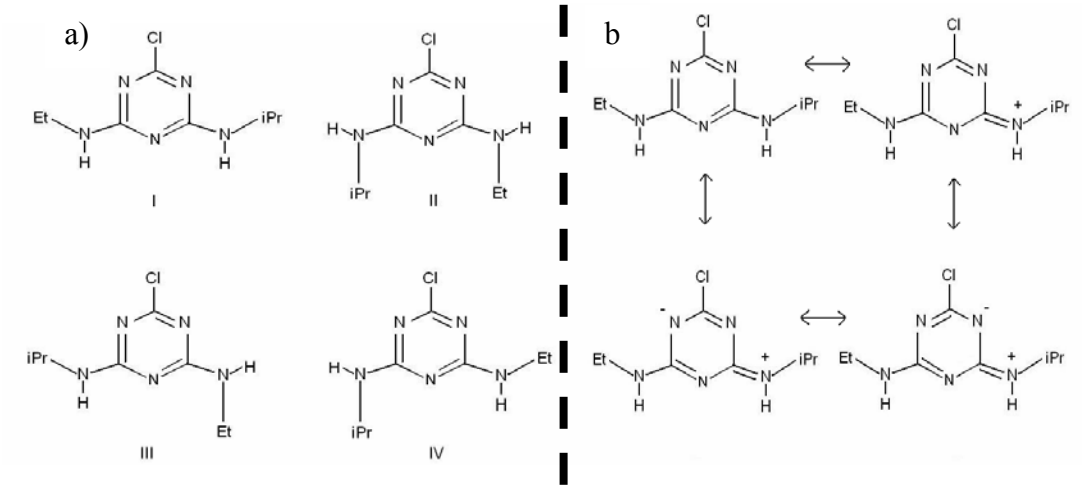

Figure 3.8. a) Conformational isomers of atrazine, b) atrazine resonance structure of conformational isomer I. Same resonance structures can de drawn for the other conformational isomers. (Et) and (iPr) denote ethyl and isopropyl respectively. Adapted from Welhouse G., and Bleam W. 1992.

To gain further insight into the SFG assignments the SSP, PPP, SPS, and PSS polarized spectra of the air – silica interface after exposure to a 0.55 mM atrazine in chloroform were acquired and are shown along with their calculated fit and component peaks in Figure 3.9 a-d.

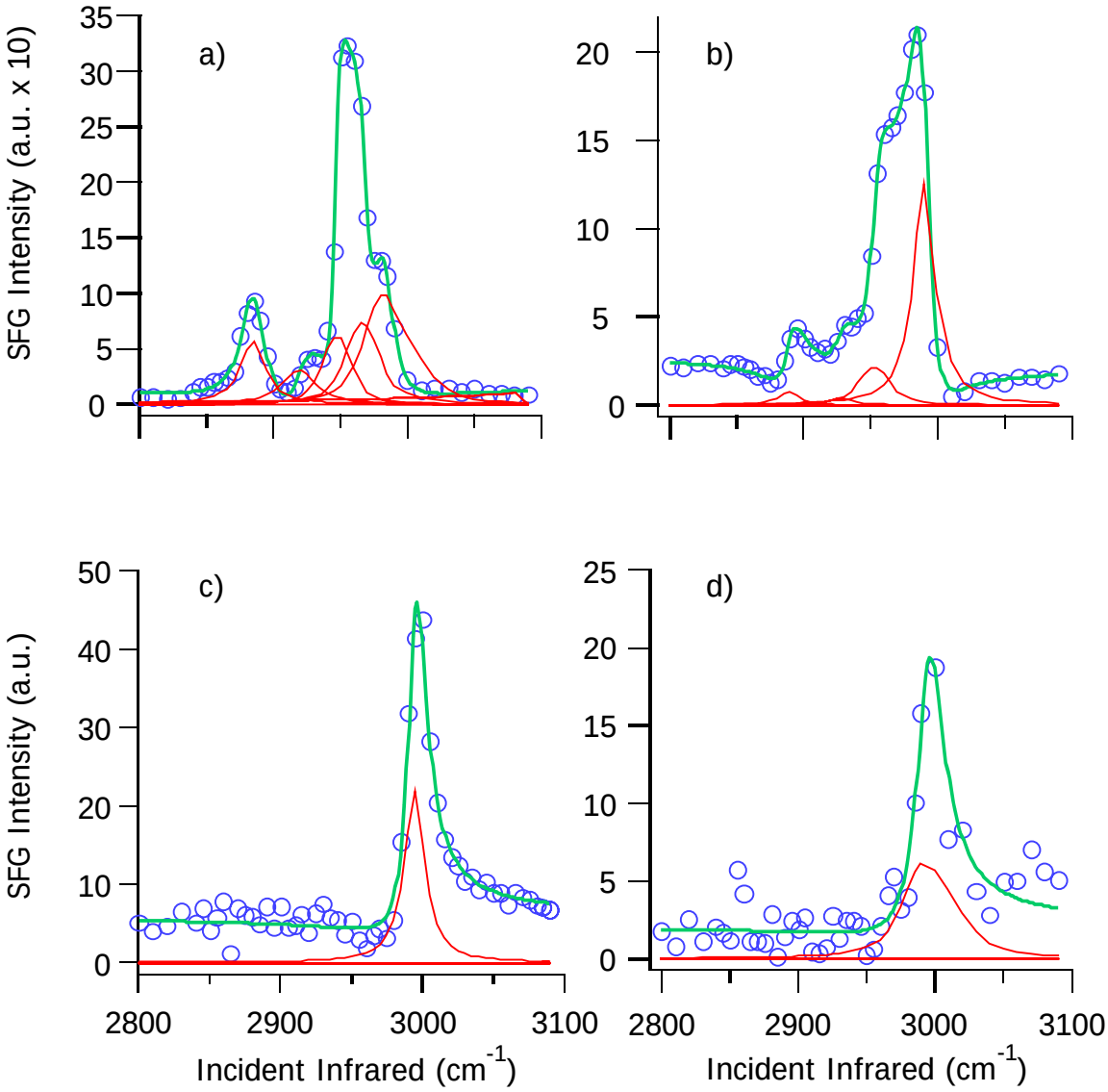

Figure 3.9. Spectral fits of SFG spectra of 0.55 mM atrazine in chloroform onto silica under different polarization combinations a) SSP, b) PPP, c) PSS, and d) SPS. The component peaks are shown in red and the calculated spectrum from the spectral fits goes through the data points.

The CH assignments previously described are consistent with the guidelines proposed by Lu R. *et al*., 2004 to assign methylene stretching modes. A summary of the peak location and the assignment of the component peaks of each polarization combination are listed in Table 3.3.

Polarization Combination				Assignment
PPP (cm^{-1})	SSP (cm^{-1})	SPS (cm^{-1})	PSS (cm^{-1})	
+ 2888	+ 2884	~	~	CH_3 ν_s
+ 2926	+ 2919	~	~	CH_2 ν_{as}
+ 2940	+ 2947	~	~	Fermi Resonance CH_3
+ 2952	- 2966	~	~	CH_3 ν_{as} in phase
- 2990	- 2983	+ 2994	+ 2994	CH_3 ν_{as} out of phase

Table 3.3. Peak position (cm^{-1}) of the SFG spectra of atrazine on silica under different polarization combinations. (~) denotes no signal, the subscript *s* denotes symmetric, *as* denotes asymmetric. (-) and (+) denotes the phase of each peak.

A significant advantage of SFG studies over Raman and infrared studies is the surface specificity. Also SFG provides information to determine molecular orientation of molecules adsorbed at the surface. In general, the molecular orientation is determined by comparing SFG intensities from different polarization combinations. (Lamber A. G., *et al* 2004) From the results shown in Table 3.3, the intensity comparison can be realized only for the methyl group. However, since two methyl groups are present in the atrazine molecule a unique tilt angle cannot be determined.

3.2.2 Atrazine interactions with the silica surface

The SSP-polarized SFG spectrum of the air – solid interface of the clean silica surface presents a weak, broad peak from at ~ 3400 cm^{-1} assigned to hydrogen bonded OH stretching bands as is shown in Fig. 3.2. The peak at ~ 3750 cm^{-1} assigned to the free OH stretching peak is observed. After the addition of atrazine to the silica surface a strong SFG response from the CH_3 stretching modes in the 2800-3000 cm^{-1} region (Fig. 3.10) and two broad peaks at ~ 3250 cm^{-1} and ~ 3440 cm^{-1} in the NH stretching region are observed (inset in Figure 3.10). The spectrum of the clean silica surface is shown for comparison. The free silanol OH stretch peak at ~ 3750 cm^{-1} is completely suppressed after the addition of the 0.55 mM atrazine in chloroform to the silica surface.

The decrease in the intensity of the peak assigned to the free OH stretch as the concentration of atrazine increases suggest that the adsorption of atrazine onto the silica surface involves the interaction of the silanol surface OH groups with atrazine.

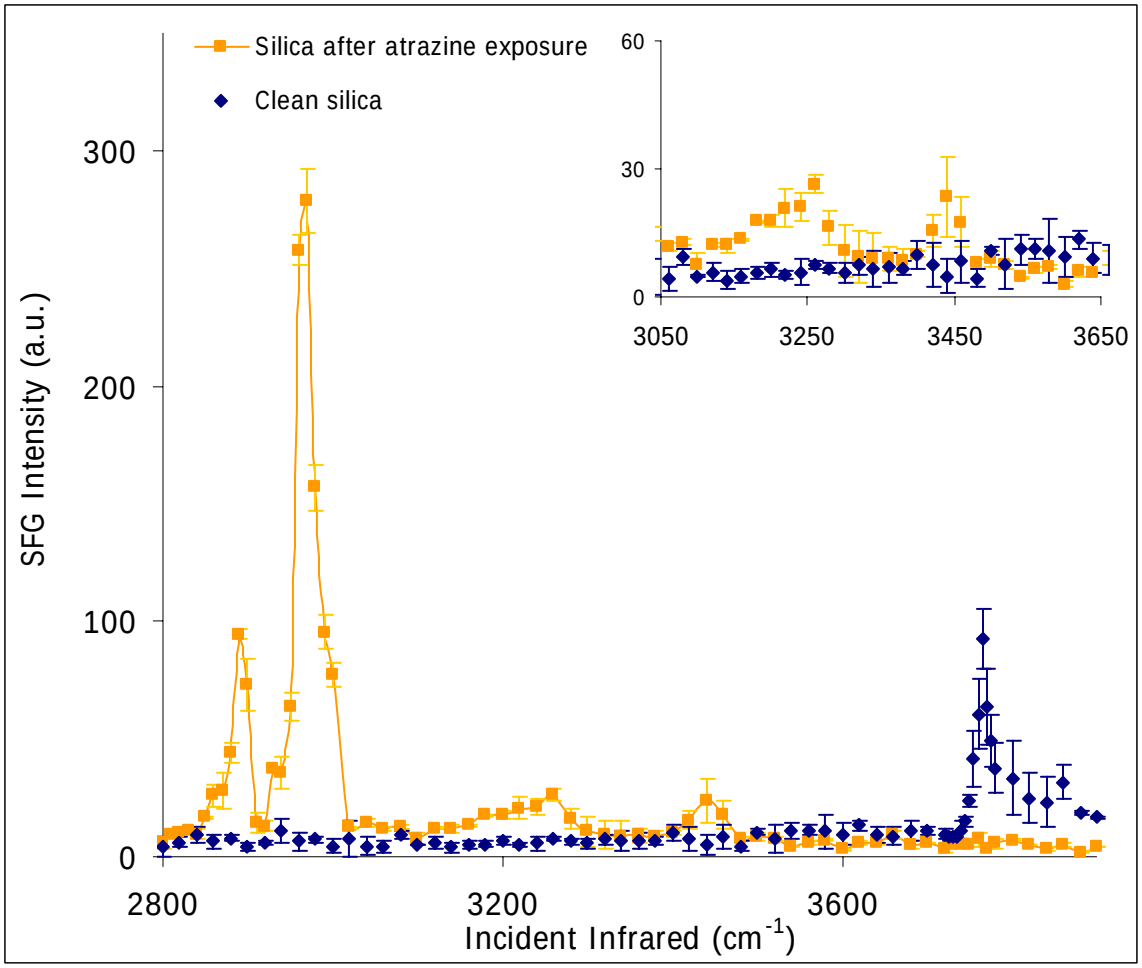

Figure 3.10. SSP-polarized SFG spectrum of the air-silica after exposure to 0.55 mM atrazine in chloroform solution. The inset shows an expanded view of the NH region. Clean silica surface is shown for comparison.

The Raman and infrared spectra of powdered atrazine (Fig. 3.5) are significantly different from the SFG spectrum of the air-silica interface after exposure to atrazine (Fig. 3.10). While Raman and infrared spectroscopies probe vibrational modes from the bulk of powdered atrazine, SFG probes vibrational modes of atrazine at the air-silica interface. Thus, observed shifts in the fundamental vibrational modes of atrazine in the SFG spectra may be due to atrazine-silica interactions. The Raman and infrared spectra of powdered atrazine show two peaks at ~ 3115 cm^{-1} and ~ 3260 cm^{-1} attributed to the bonded NH, and the free NH, respectively. In the SFG spectrum of the silica surface after the addition of atrazine, the NH vibrational modes are shifted to higher frequencies ~ 3250 cm^{-1} and ~ 3440 cm^{-1}.

Although the NH stretching is a highly localized mode, it is expected to shift its frequency if changes in the environment of the NH occur. (Mirkin N., *et al* 2004) Shift in frequencies of the NH stretching mode have been reported to be as large as 150 cm^{-1}. (Bellamy L., 1980) Therefore, the blue shift observed of the NH stretch can be attributed to the variations in the environment surrounding the NH groups of atrazine. From these results, it is proposed that the atrazine-silica interaction involves NH groups from atrazine and OH groups from the silica surface.

In situ FTIR spectroscopy studies have shown that at the silica surface there is only hydrogen bond formation between surface silanol OH groups and weakly basic molecules. (Zaki M. *et al* 2000, Zaki M. *et al* 2001, Dines T. *et al* 2002, Dines T. *et al* 2003) The hydrogen-bonding propensity of atrazine has been determined by NMR

studies. Atrazine molecules are able to accept hydrogen bonds from phenol, trifluoroethanol and hexafluoro-2-propanol, and donate to dimethyl sulfoxide, and acetone. (Welhouse G., and Bleam W. 1993) Therefore, in this study hydrogen bonding is the proposed mechanism of the interaction between atrazine and the surface silanol OH groups.

To aid in obtaining information about the interactions between atrazine and the surface silanol OH groups a series of experiments were performed and are presented in the following section.

3.2.3 Strength of the atrazine-silica interaction

To examine the atrazine-silica interaction, the SFG spectrum of the air-silica interface after exposure to the 0.55 mM atrazine in chloroform solution was again acquired, Fig 3.11 a. The silica surface was then rinsed with nanopure water for 30 min, and a second SFG spectrum was acquired, Fig. 3.11 a. The SFG spectrum of the clean silica is shown for comparison.

The peaks attributed to atrazine decreased in intensity after rinsing the silica surface, Fig. 3.11 c. An enhancement in the intensity of the free silanol OH peak after water rinsing relative to that of the before rinsing is also observed, Fig. 3.11 b. This suggests that atrazine was removed from the silica surface by water rinsing. Therefore, the atrazine adsorption on the silica surface must involve relatively weak physical forces. The SFG spectrum of air-silica interface after rinsing is similar to that obtained by

exposing the silica surface to water, Fig. 3.2 a. This is consistent with water molecules hydrogen bonded to the surface silanol OH groups of silica as proposed in section 3.1.

There are two possible mechanisms for the removal of atrazine from the silica surface. First, a displacement of atrazine molecules by water molecules can occur. This is based on the fact that water molecules have a higher affinity for the silica surface silanols than atrazine molecules. The second possible mechanism involves solvation of atrazine by water prior to atrazine desorption from the silica surface.

In summary, the proposed hydrogen bonding mechanism of interaction between atrazine and the surface silanol OH groups is confirmed.

These results are consistent with studies of sorption isotherms of atrazine on smectites, kaolinite, and montmorillonite reported by Barriuso E., *et al* 1994, Herwing U., *et al* 2001, Clausen L., *et al* 2001, Davies E. and Jabeen N., 2003.

The pH of the solutions (pH ~ 6) used in the experiments of this thesis work suggests that atrazine (pKa_1 of 1.60 and pKa_2 of 1.95) is adsorbed on the silica surface (pKa_2 of 4) as a neutral molecule. However, the adsorption of protonated atrazine has been proposed in sorption-desorption studies when the pH of the clay suspension is substantially greater than the equilibrium constant *pKa*. (Ainsworth C., *et al* 1987) This phenomenon is attributed to the presence of adsorbed inorganic cations on clay surfaces. Protonated atrazine species were adsorbed through cation exchange, which involves

stronger interactions than hydrogen bonds. (Barriuso E., *et al* 1994) Therefore, since in this thesis work inorganic cations are not present at the silica surface and desorption of atrazine was completed by water dilution, the possibility of having protonated atrazine molecules at the silica surface was not considered.

A schematic of the sequence followed in this experiment to examine the atrazine-silica interaction is shown in Figure 3.12. The air-silica interfaces before and after atrazine addition are shown in Fig 3.12 I and II respectively. The atrazine exposed silica surface after water rinsing is depicted in Figure 3.12, III. Different atrazine orientations relative are proposed relative to the surface plane and depicted in Figure 3.12 II.

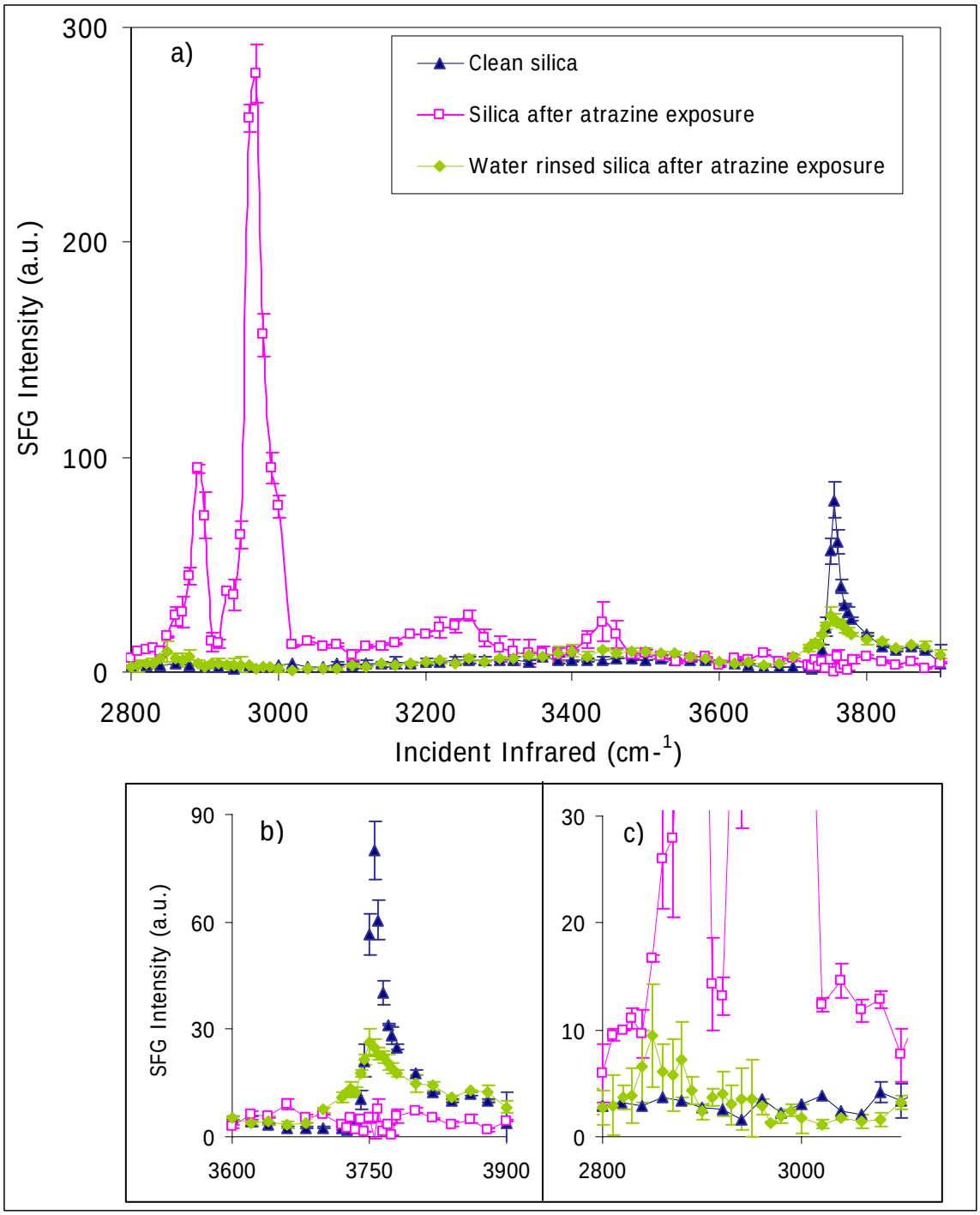

Figure 3.11 a) SFG spectra of the air-silica interface followed to atrazine exposure before and after water rinsing are shown in open pink squares and green solid diamonds, respectively. The spectrum of the clean silica is shown in open blue triangles for comparison. The insets show an expanded view of b) the free silanol OH stretch region, and c) the CH stretching region (2800 - 3100 cm^{-1}).

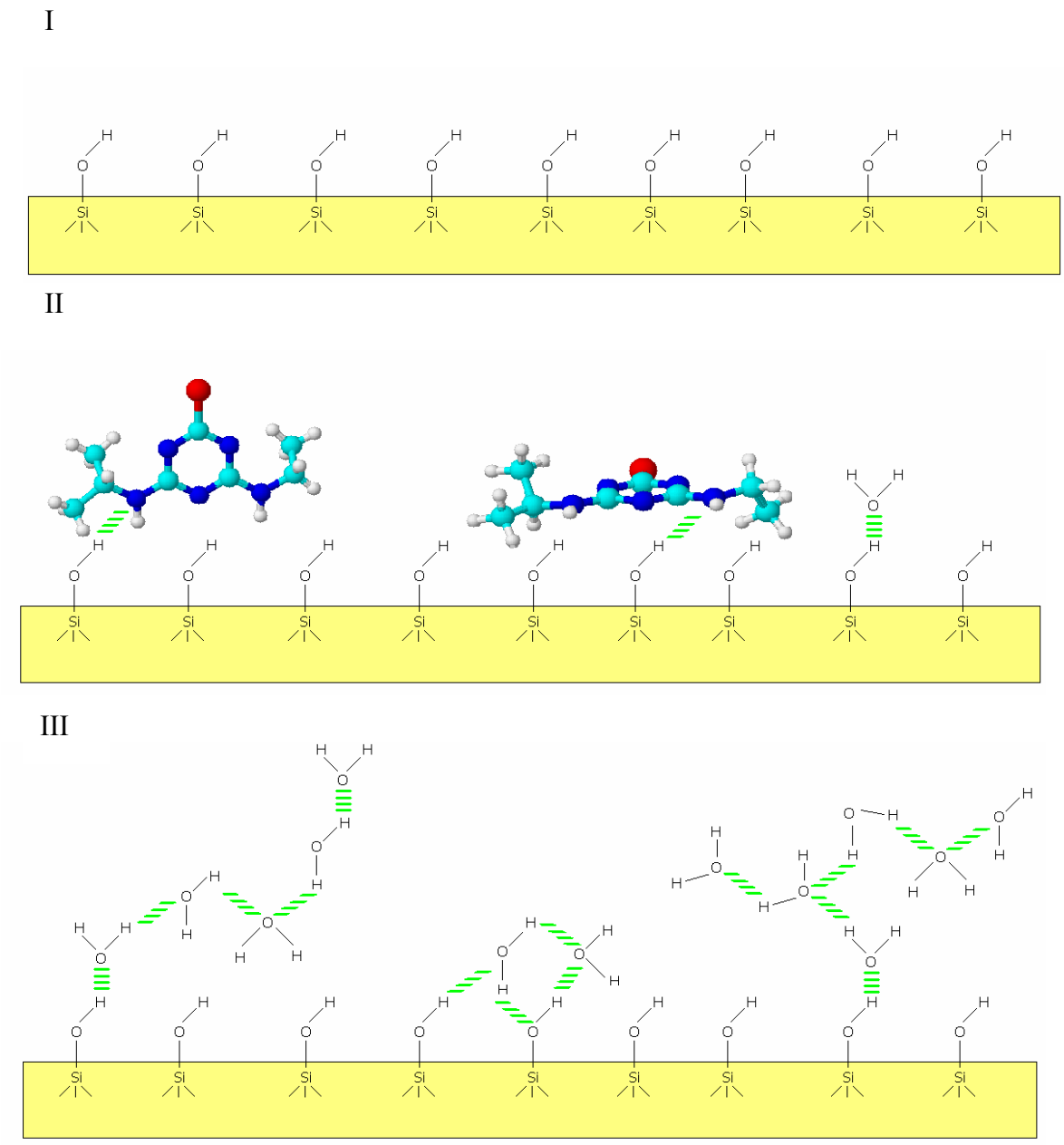

Figure 3.12. Schematic of the sequence followed in the water-rinsed experiment. The air-silica interfaces before and after atrazine addition are shown in I and II, respectively. The atrazine exposed silica surface after water rinsing is depicted in III. In II, red spheres are chlorine atoms, light blue spheres are carbons atoms, dark blue spheres are nitrogen atoms, and gray spheres are hydrogen atoms of the atrazine molecules.

It was previously demonstrated that chloroform did not interact with the surface silanol OH groups on the silica surface (Section 3.1, Fig. 3.2 c). Therefore, chloroform was chosen as the rinsing solvent to obtain a better understanding of the atrazine affinity to the surface silanol OH groups. The silica plate after atrazine exposure was placed in 100 mL of neat chloroform solution. The chloroform solution was stirred for 30 min. SFG spectra before and after the chloroform rinsing were acquired, and are shown in Figure 3.13. The clean silica surface is also shown for comparison.

Consistent with the water-rinsed silica surface, the chloroform-rinsed silica surface SFG spectrum shows a peak vanishing in the CH_3 stretching (~ 2900 cm^{-1}) region, Fig. 3.13 a-c, and in the NH (~ 3250 cm^{-1} and ~3440 cm^{-1}) region, Fig. 3.13 a, confirming the weak interaction between atrazine and the surface silanol OH groups. Additionally, an enhancement in the intensity of the free silanol OH peak after chloroform rinsing relative to that of the before rinsing is also observed, Fig. 3.13 b. However, the original intensity of the free silanol OH peak did not return after chloroform rinsing procedure. This interesting feature was not expected since no interaction of chloroform and the silica surface was found in an earlier experiment (section 3.1, Fig. 3.2 c) In these experiments the silica surface was exposed to neat chloroform by passing ~ 300 μL^{-1} of it over the silica surface (~ 10 sec contact time), while in the chloroform rinsing procedure the silica surface was in contact with chloroform for 30 min. To understand this discrepancy a clean silica plate was placed in a neat chloroform solution for 30 min under constant stirring. The SFG spectrum of the air- silica interface after 30 min of chloroform rinsing was acquired and is shown in Figure 3.14. The SFG spectra of the air-silica interface after

30 min of chloroform rinsing after atrazine exposure, and the clean silica are shown for comparison.

In the SFG spectrum of the air- silica interface after 30 min of chloroform rinsing a decrease in the free silanol OH peak (3750 cm^{-1}) is observed as compared to that of the clean silica. This result suggests that chloroform interacts with the surface silanol OH groups after 30 min of contact, likely through hydrogen bonding. Additionally, a small enhancement in the CH stretching region (2800 to 3100 $cm^{-1)}$ is observed. As mentioned previously, no interaction was found between chloroform and surface silanol OH group under ~ 10 sec contact time (section 3.1, Fig. 3.2 c), whereas a hydrogen bonding mechanism was proposed between the surface silanol OH groups with water and under those same experimental conditions. This can be explained by the fact that chloroform is less effective in forming hydrogen bonds than water.

In the SFG spectrum of the air- silica interface of the chloroform-rinsed silica after atrazine exposure, the intensity of the free silanol OH peak (3750 cm^{-1}) falls within experimental error of the intensity of free silanol OH peak of the chloroform-rinsed silica spectrum. These results suggest that chloroform interacts with the silica surface after longer exposure times.

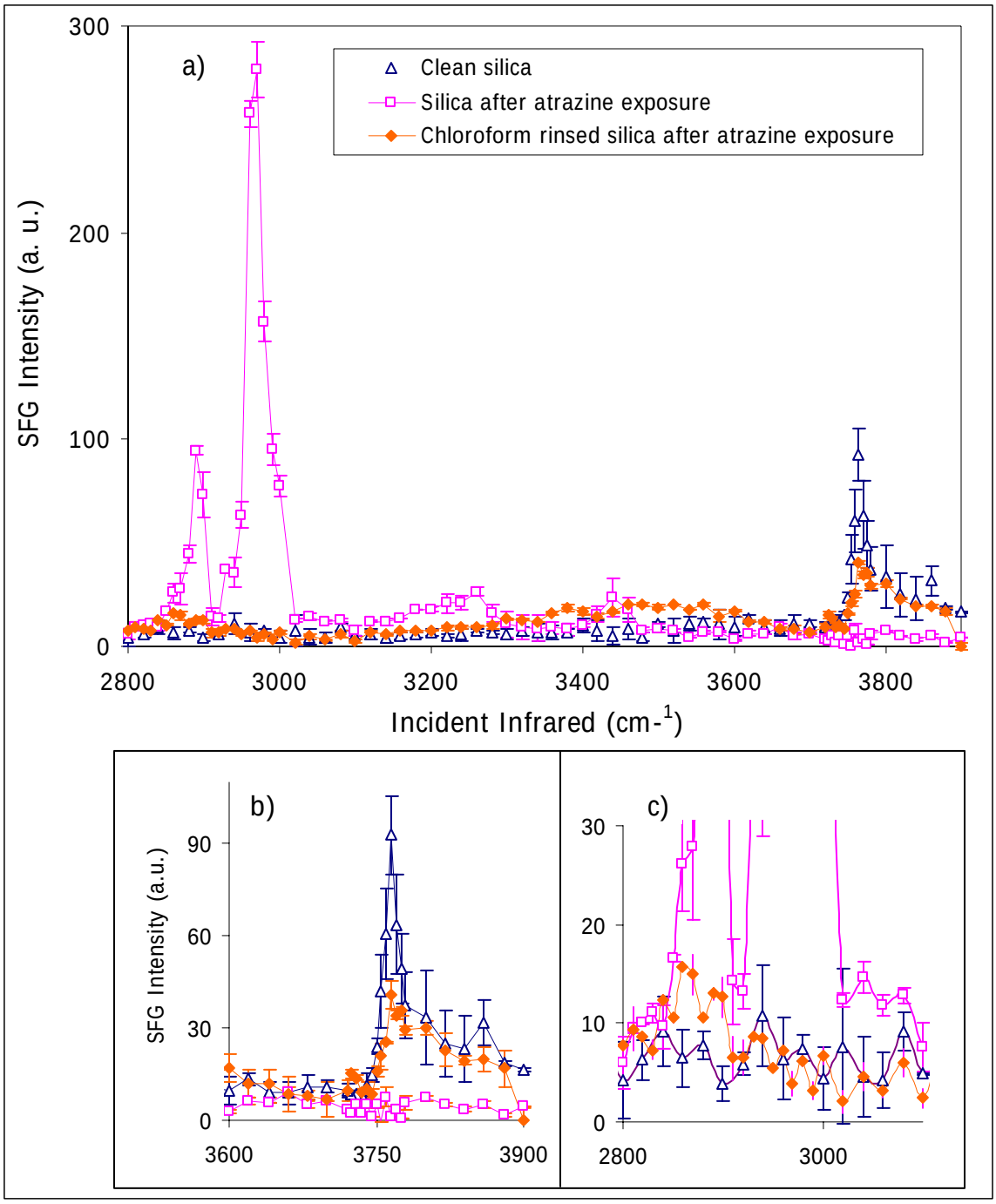

Figure 3.13. a) SFG spectra of the air-silica interface after atrazine exposure before and after chloroform rinsing are shown in open pink squares and solid orange diamonds, respectively. The spectrum of the clean silica is shown in blue triangles for comparison. The insets show an expanded view of b) the free silanol OH stretch region, and c) the CH stretching region (2800 - 3100 cm^{-1}).

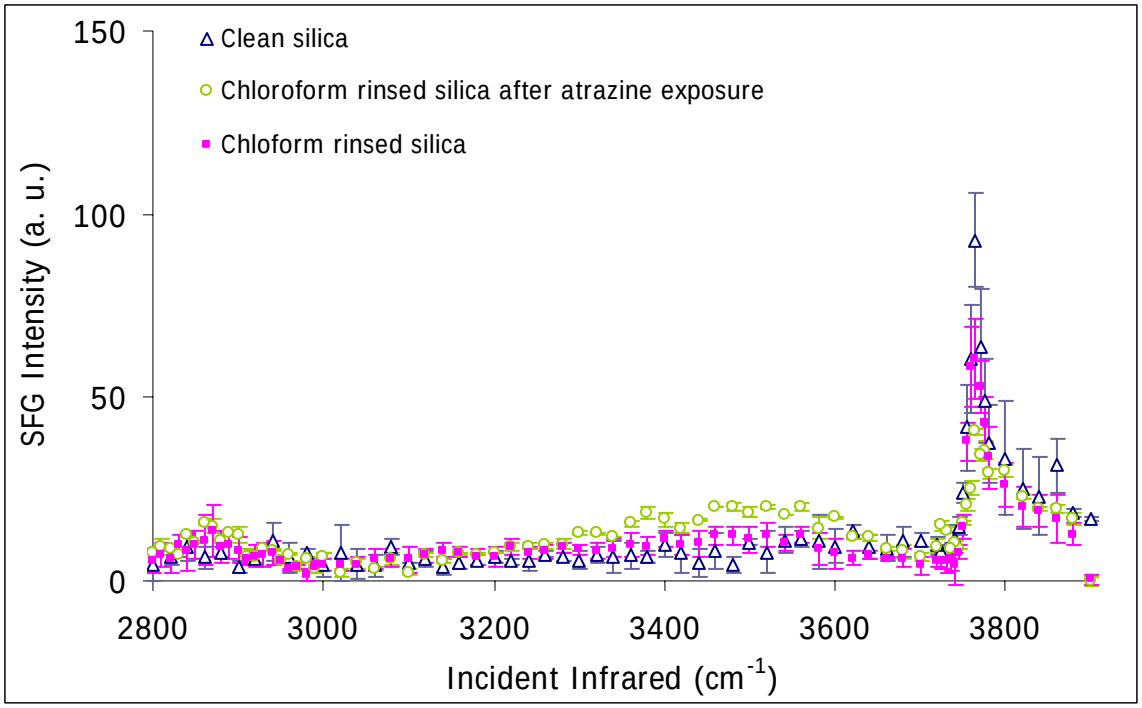

Figure 3.14. SFG spectra of the air-silica interface after 30 min of chloroform rinsing before and after atrazine exposure are shown in solid pink squares and open green circles, respectively. The spectrum of the clean silica is shown in blue triangles for comparison.

The atrazine removal from the silica surface after chloroform rinsing can be attributed to two possible reasons. Atrazine molecules may be solvated by chloroform and thereby removed from the silica surface. A second reason for the atrazine desorption is attributed to a displacement of atrazine by chloroform.

Atrazine, a weakly polar molecule, is highly soluble in chloroform (52 g L^{-1} at 25 °C) and sparingly soluble in water (33 mg L^{-1} at 25 °C). Chloroform shows low affinity for the silica surface, whereas water reveals high affinity for silica surface. Solvent affinity for the silica surface and solvation of the solute contribute to atrazine desorption.

In order to elucidate which mechanism has the largest impact on atrazine desorption, a new solvent with intermediate silica affinity and atrazine solubility could be evaluated. This is suggested for the future work, e.g. the use of acetonitrile as the solvent.

CHAPTER 4

CONCLUSIONS

The air-silica interface after exposure to atrazine was investigated using sum frequency generation spectroscopy. Atrazine interacts with the surface of silica through hydrogen bonding of the amine moieties and the silanol OH groups. Molecular displacement and solvation mechanisms may contribute to the atrazine desorption from silica. Hydrogen bonding interactions suggest that atrazine, once adsorbed onto the clay fraction of soils, is easily desorbed. Atrazine can then be transported deeper into the soils, and ultimately into the ground water. This proposed hydrogen-bonding mechanism is consistent with previous studies of atrazine sorption on clay minerals.

Air-silica interfaces after exposure to water, methanol, and chloroform were also analyzed. Water molecules interact with the surface silanol OH groups through hydrogen bonding. Chloroform was less effective than water at interacting with the silanol OH groups at the silica surface.

CHAPTER 5

FUTURE WORK

There are four recommended experiments to provide further insight this thesis work: 1) analysis of the air-silica interface after methanol and after atrazine in chloroform solution exposure should be completed under 0% RH conditions to eliminate water competition for the silica surface binding sites, 2) acetonitrile should be used in the atrazine desorption procedure to evaluate which mechanism prevails, molecular displacement or solvation of atrazine; however, it is possible that both mechanisms play a significant role in the atrazine desorption process, 3) lower pH conditions in the atrazine solution have to be tested to induce atrazine protonation at the silica surface and to evaluate the strength of this interaction, and 4) to fully evaluate the ability of atrazine to migrate through soil, the binding mechanism of the degradation products of atrazine, ADE and ADI, need to be evaluated.

REFERENCES

Abraham M. H., Grellier P. L., Prior D. V., Duce P. "Hydrogen bonding. Part 7. A scale of solute hydrogen-bond acidity based on log k values for complexation in tetrachloromethane". *Journal of Chemical Society Perkin Transcripst II* . **1989**, 699-711.

Ainsworth C., Zachara J., Schmidt R. "Quinoline sorption on Na-montmorillonite: contributions of the protonated and neutral species". *Clays Clay Minerals*. **1987,** 35:121-128.

Almeida De W., Malley O. "An AM1 study of conformational preference for the herbicide atrazine". *Journal of Molecular Structure (Theochem)*. **1992**, 253:349-356.

Allen H. C., Raymond E. A., Richmond G L. "Surface Structural Studies of Methanesulfonic Acid at Air /Aqueous Solution Interfaces Using Vibrational Sum Frequency Spectroscopy". *Physical Chemistry A*. **2001,** 105:1649-1655.

Allen H. C., Raymond E. A., Richmond G L. "Non-linear vibrational sum frequency spectroscopy of atmospherically relevant molecules at aqueous solution surfaces" *Current Opinion in Colloid & Interface Science*. **2000**, 5: 74-80

Alvey S., Crowley D. E. "Survival and activity of an atrazine-mineralizing bacterial consortium n rhizosphere soil". *Environmental Science and Technology*. **1996**,30(5):1596-1603.

Armstrong D.E., Chester C., Harris J H. "Atrazine hydrolysis in soil" *Soil Science Society of American Proc*. **1967**,31:61-66.

Bain, C. D. "Sum Frequency Vibrational Spectroscopy of the Solid-Liquid Interface". *Chemical Society Faraday Transitions*. **1995**, 91:1281-1296.

Barriuso E., Laird D., Koskinen C., Dowdy R. "Atrazine desorption from smectites". *Soil Science Society of American*. **1994,** 58:1632-1638.

Barriuso E., Bacr U., Calvet R. "Dissolved organic matter and adsorption-desorption of dimefuron, atrazine and carbetamide by soils". *Journal of Environmental Quality*. **1992**, 21:359-367.

Bass J. and Duyzer J., "Concentrations of pesticides in air and rainwater. A pilot study into concentrations of pesticides in air and rainwater in Naaldwijk, de Zilk and site Noodwijk (in Dutch), report R97/113, TNO Institute of Environmental Sciences, Energy Research and Process Innovation, Apeldoorn, **1997** p 52.

Bellamy L. The infrared spectra of complex molecules. Chapman and Dall. London, New York, 1975.

Bellamy L. Advances in infrared group frequencies. 2nd Edit. Chapman and Dall. London, New York, 1980.

Bergman, D.L., Laaksonen, L., and Laaksonen, A. "Visualization of solvation structures in liquid mixtures". *J. Mol. Graph. Model.* **1997**, 15**:** 301-306

Buck U., Ettischer I., Melzer M., Buch V., Sadlej J. "Structure and spectra of three-dimensional (H2O)n clusters, n=8, 9, 10". *Physical Review Letters* .**1998**, 80:399-406.

Calvet R. Adsorption-desorption phenomena. Academic press. **1980**.

Cardenas J. "Surface charge of silica determined using X-ray photoelectron spectroscopy". *Colloids and Surfaces. A*. **2004**, 252:213-219.

Celis, R.; Cornejo, J.; Hermosin, M. C.; Koskinen, W. C "Sorption-desorption of atrazine and simazine by model soil colloidal components". *Soil Science Society of America Journal*. **1997**, 61: 436-443.

Cerejeira M. J., Viana P., Batista S., Pereira T., Silva E, Valerio M. J., Silva A., Ferreira M, Silva-Fernandes A.M. "Pesticides in Portuguese surface and ground waters". *Water Research*. **2003**, 371055–371063.

Chiou C., Peters L. J., Freed V.H.A. "A physical concept of soil-water equilibria for nonionic organic compounds". *Science*. **1979**, 206:831-832.

Chuang I.-S., Maciel G. E., "Probing Hydrogen Bonding and the Local Environment of Silanols on Silica Surfaces via Nuclear Spin Cross Polarization Dynamics" *Journal of the American Chemical Society*. **1996**, 118:400-407.

Clausen L., Fabricius I., Madsen L. "Adsorption of pesticides onto quartz, calcite, kaolinite, and α-alumina". *Journal Environmental Quality*. **2001,** 30:846-857.

Colombini M. P., Fuoco R., Giannarelli S., Pospísil L trsková. "Protonation and degradation reactions of s-Triazine herbicides" *Microchemical Journal.* **1998**, 59:239-245.

Comber S.D.W. “Abiotic persistence of atrazine and simazine in water”. *Pesticide Science*. **1999**, 55:696-702.

Davies E., and Jabeen N. “The adsorption of herbicides and pesticides on clay minerals and soils. Part 2. Atrazine” *Journal of Inclusion Phenomena and Macrocyclic Chemistry.* **2003**, 46:57-64

Devlin J. P., Sadlej J., Buch V. “Infrared Spectra of Large H2O Clusters: New Understanding of the Elusive Bending Mode of Ice”. *Physical Chemistry A*. **2001**, 105:974-983.

Dines T. J., MacGregor L. D., Rochester C.H. “IR spectroscopy of N-Methylpyrrole adsorbed on oxide. Probe of surface acidity”. *Journal Colloidal interfacial science*. **2002**, 245:221-228.

Dines T. J., MacGregor L. D., Rochester C.H. “Adsorption of 2-Chloropyridine on oxides. An infrared spectroscopy study”. *Spectrochemical Acta, Part A*. **2003,** 25:3205-3210.

Dixon J., and Weed S. Minerals in soils environments. Soil Science Society of America, Madison Wisconsin, USA. **1989**.

Du Q., Freysz E., Shen Y. R. “Vibrational spectra of water molecules at the quartz/water interfaces” *Physical Review Letters* **1994**, 72:238241.

Du Q., Superfine R., Freysz E., Shen Y R. “Vibrational spectroscopy of water at the vapor/water interface”. *Physical Review Letters* **1993**, 70:2313-2316.

Duval Y, Mielczarski J. A., Pokrovsky O. S, Mielczarski E., Ehrhardt J. J. “Evidence of the Existence of Three Types of Species at the Quartz-Aqueous Solution Interface at pH 0-10: XPS Surface Group Quantification and Surface Complexation Modeling**”.** *Journal of Physical Chemistry B.* **2002**, 106(11): 2937-2945.

Erickson E. E., Lee K. H. “Degradation of atrazine and related *s*-triazines”. *Critical review in environmental control.* **1989**, 19:1-14.

EPA, US Environment Protection Agency: Interim “Reregistration Eligilibility Decision for Atrazine” (IRED) Case No. 0062 , January **2003**.

Frisch M., Trucks G., Schlegel H., Scuseria G., Robb M., Cheeseman J., Montgomery J., Vreven T., Kudin K., Burat J., Millam J., Iyengar S., Tomasi J., Barone V., Mennuci B., Cossi M., Scalmani G., Rega N., Peterson G., Nakatsuji H., Hada M., Ehara M., Toyota K., Fukuda R., Knox J., Adama C., Jaramillo J., Ayala P., Foresman J., Wong M., Gonzalez C., Pople J. A. *Gaussian 03*, revision B.04; Gaussian, Inc:Pittsburg, PA, 2003.

Garmouna M., Blanchoud H., Teil M., Blanchard M., Chervreuil M. "Triazines in the Marne and the Seine rives (France): longitudinal evolution and flows". *Water, Air, and Soil Pollution.* **2001**, 132(1-2): 1-17.

Goldberg M C., Cunningham K. >, Squillace P. J. "Photolytic degradation of atrazine in the Cedar river, Iowa, and its tributaries". In U.S. Geological Survey Toxic Substances Hydrology Program –Proceedings of the Technical Meeting; Mallard, G. E. Aronson D., Eds, Monterey, CA; U.S. Geological Survey, Water-Resources. Investigation Report. **1991**, 91-4034.

González-Prada E., Socías-Viciana M., Saifi M., Ureña-Amate M., Flores-Céspedes F., Fernández-Pérez M., Villafranca-Sánchez M. "Adsorption of Atrazine from aqueous solution on heat treated kerolites". *Chemosphere.* **2003,** 51:85-93.

Gragson D. E., MacCarty B. M., Richmond G. L. "Ordering of interfacial water molecules at the charged air/water interface observed by Vibrational Sum Frequency Generation". *Journal of American Chemical Society.* **1997**, 119:6144-6152.

Guyot P., Hunt J., Shen Y. R. "Sum frequency of a Langmuir film: study of molecular orientation of a two-dimensional system". *Physical Review Letters*. **1987**, 59:1597-1600.

Hasset J., Banwart W., Wood S., Means J. "Sorption of α-naphthol: Implications concerning the limits of hydrophobic sorption". *Soil Science Society of American.* **1981,** 45:38-42.

Hiemstra T., Yong H., van Riemsdijk W. H. "Interfacial charging phenomena of aluminium (hydro) oxides". *Langmuir*. **1999**, 15:5942.

Hert W. "Infrared frequency shifts due to hydrogen bonding of surface amino groups on silica". *The Journal of Physical Chemistry*. **1973**, 77:1473-1474.

Herwig U., Klumpp E., Narres H., Schwuger J. "Physicochemical interactions between Atrazine and clay minerals". *Applied Clay Science.* **2001,** 18:211-222.

Hirose C., Akamatsu N., Domen K. "Formulas for the analysis of the surface SFG spectrum and transformation coefficients of Cartesian SFG tensor components". *Applied Spectroscopy*. **1992**, 46:1051-1072.

Hommel E.L, Allen H. C. "The air – liquid interface of benzene, toluene, m-xylene, and mesitylene: a sum frequency, Raman, and infrared spectroscopic study". *Analyst*. **2003**, 128:750-755.

Iler R. K. The chemistry of silica: solubility, polimerization, colloid and surface properties, and biochemistry. Willey-Interscience Publication. John Wiley and sons. New York, **1979**.

Islam, M. Omedul; Hara, Masayuki; Miyake, Jun. "Induction of P-glycoprotein, glutathione-S-transferase and cytochrome P450 in rat liver by atrazine" *Environmental Toxicology and Pharmacology.* **2002**, 12(1); 1-6.

Karickhoff S., Brown D., Scott T. "Sorption of hydrophobic pollutant on natural sediments". *Water Research.* **1979,** 13: 241-248.

Konstantinou I., Triantafyllos A., Petrakis D., Pomonis P. "Removal of herbicides from aqueous solutions by adsorption on Al-pillared clays, Fe-Al pillared clays and mesoporous alumina aluminum phosphates". *Water Research.* **2000,** 3(12): 3123-3136.

Laaksonen L. "A graphics program for the analysis and display of molecular dynamics trajectories". *J. Mol. Graph.* **1992**, 10: 33-34.

Langmuir D. Aqueous Environmental Geochemistry. 1st ed: Pearson Education. 1997.

Laird D. A., Barriuso E., Dowdy R. H., Koskinen W. C. "Adsorption of atrazine on Smectites" *Soil Science Society of American.* **1992,** 56:62-67.

Laird D. A., Yen P., Koskinen W., Steinhelmer T., Dowdy R. "Sorption of atrazine on soils clay components" *Environmental Science and Technology*. **1994,** 28:1054-1061.

Larkin P. J., Makowski M. P., Colthup N. B., Flood L. A. "Vibrational analysis of some important group frequencies of melamine derivatives containing methoxymethyl, and carbamate substituents: mechanical coupling of substituent vibrations with triazine ring modes". *Vibrational Spectroscopy*. **1998**, 17: 53-72.

Le Pennec, G.; Le Pennec, M "Evaluation of the toxicity of chemical compounds using digestive acini of the bivalve mollusc Pecten maximus L. maintained alive in vitro" *Aquatic Toxicology.* **2001**, 53(1), 1-7.

Lesan H., Bhandari A. "Atrazine sorption on surface soils: time-dependent phase distribution and apparent desorption hysteresis". *Water Research.* **2003,** 37:1644-1654

Lerch R., Thurman E., Kruger E. "mixed-Mode sorption of Hydroxylated Atrazine degradation products to soil: A mechanism for bound residue". *Environmental Science and Technology*. **1997**, 31:1539-1546.

Li H. C., De Bruyn P. L. **"**Electrokinetic and adsorption studies on quartz". *Surface Science*. **1966**, 5:203-220.

Li H., Sheng G., Teppen B., Johnson C., Boyd S. 'Sorption and desorption of pesticides by clay minerals and humic acid-clay complexes. *Soil Science Society of American*. **2003,** 67:122-131.

Lin-Vien D., Colthup N., Fately W., Grasselli J. The Handbook of Infrared and Raman characteristic frequencies of organic molecules. Academic Press. New York, 1991.

Lode O., Eklo O M., Holen B., Svenson A., Johnsen A M. "Pesticides in precipitation in Norway". *Science of Total Environment*. **1995,** 160/161, 421-431.

Lu R., Gan W., Wu B., Chen H., Wang H. "Vibrational polarization spectroscopy of CH stretching modes of the Methylene group at the vapor/liquid interfaces with Sum Frequency Generation" *Journal Physical Chemistry B***. 2004**,108:7297-7306.

McCreery, R. L. Raman Spectroscopy for Chemical analysis; John Wiley and sons. New York, **2000**

Messmer M. C., Conboy J. C., Richmond G. L. "Observation of molecular ordering at the liquid-liquid interface by resonant sum frequency generation". *Journal of American Chemical Society.* **1995**, 117:8039-8040.

Meyer M T., Thurman E. M. Herbicides Metabolites in surface waters and groundwater. ACS Symposium Series. Washington DC.**1996.**

Miranda P., Shen Y. "Liquid interfaces: a study by Sum Frequency Vibrational Spectroscopy". *Journal Physical Chemistry B***. 1999**,103:3292-3307.

Miller S. M., Sweet C W., Depinto J. V., Hornbuckle K "Atrazine and nutrients in precipitation: results from the lake Michigan mass balance study". *Environmental Science and Technology*. **2000,** 34(1): 55-61.

Moore, A.; Lower, N. "The impact of two pesticides on olfactory mediated endocrine function in mature male Atlantic salmon(*Salmo salar* L.)" *Comparative Biochemistry and Physiology, Part B: Biochemistry & Molecular Biology.* **2001**, 129:269-276.

Morrow B. A., McFarlan A. J. "Chemical reactions at the silica surfaces". *Journal Non-crystals solids*. **1990**,120(1-3) 61-70.

Murphy W. F., Zerbetto F., Duncan J.L., McKean D. C. " Vibrational spectrum and harmonic force field of trimethylamine". *Journal of Physical Chemistry*. **1993**, 97:581-595.

Myneni S.C. B., "Soft X-ray spectroscopy and spectromicroscopy of organics molecules in the environment". *Reviews Mineral Geochemistry*. **2002**, 49, 485-495.

NIST, Standard Reference Data Program. Collection (C) 2003 copyright by the U.S. Secretary of Commerce on behalf of the United States of America. All rights reserved.

Parks G.A. "Surface and interfacial free energy of quartz". *Geophysical Resources.* **1984,** 89:3997-4008

Pereira W. E., Rostad C. E. "Occurrence, distributions and transport of herbicides and their degradation products in the lower Mississippi River and its tributaries". *Environmental Science and Technology*. **1990,** 24 (9): 1400-1406.

Pribble R. N., Zwier T. S. "Size-specific infrared spectra of benzene-(H2O)n clusters (n = 1 through 7): evidence for noncyclic (H2O)n structures". *Science*. **1994**, 265:75-79.

Protzman R. S., Lee P. H., Ong S. K., Moorman T. B. "Treatment of formulated Atrazine rinsate by Agrobacterium radiobacter strain J14A in a sequencing batch biofilm reactor". *Water Resources*. **1999,** 33:1399-1404.

Rablen P., Lockmna J., Jorgensen W. "*Ab initio* study of Hydrogen-bonded complexes of small organic molecules with water". *Journal of Physical Chemistry A*. **1998**, 102:3782-3797.

Ralebitso T.K., Senior E., Van Verseveld H. W. "Microbial aspects of Atrazine degradation in natural environments". *Biodegratation*. **2002,** 13:11-19.

Ren J., Jiang K. "Impact of atrazine on the water resources of the Yang river in Zhangjiakou area in China". *Bulletin of Environmental Contamination and Toxicology*. **2002**, 68(6): 893-900.

Sawhney B., Singh S. "Sorption of atrazine by Al- and Ca- saturated smectite". *Clays Clay Minerals*.**1997,** 45:333-338.

Schnnitzer C., Baldelli S., Campbell D. J., Shultz M J. "Sum Frequency Generation of O-H Vibrations on the Surface of H2O/HNO3 Solutions and Liquid HNO3". *Physical Chemistry A*. **1999***,* 103:6383-6386.

Shen Y. R."Surface properties probed by Second-Harmonic and Sum Frequency Generation". *Nature*. **1989**, 337,519-525.

Shen Y. R. The principles of nonlinear optics. John Wiley &sons: New York, **1984**.

Sheng G., Teppen B., Johnson C., Boyd S. "Potential contributions of smectite clays and organic matter to pesticide retention in soils". *Journal of Agriculture, Food, and Chemistry*. **2001**,49:2899-2907.

Shultz M. J., Baldelli S., Schnnitzer C., Simonelli D. "Aqueous Solution/Air Interfaces Probed with Sum Frequency Generation Spectroscopy". *Physical Chemistry B*. **2002,** 106:5313-5324

Sposito G. Chemical equilibria and kinetics in Soils. Oxford University Press, New York **1994**

Stumm W., Morgan J. J. Aquatic Chemistry. 3rd ed. New York: John Wiley and Sons. **1996**.

Tuel A., Hommel H., Legrand A. P., Kovats E. "A silicon-29 NMR study of the silanol population at the surface of derivatized silica". *Langmuir* **1990**, 6; 770-775

Van Roosmalen A. J., Mol J. C. "An infrared study of the silica gel surface. 1. Dry silica gel". *Physical Chemistry*. **1978**, 82; 2748-2751.

Verstraeten I M., Carr J. D., Steele G. V., Thurman E. M., Bastian K. C., Dormedy D. F., "Surface water-groun water interaction: herbicide transport into municipal collector wells". *Journal Environmental Quality*. **1999,** 28(5): 1396-1405.

Walrafen G. E., Chu Y. C. "Linearity between Structural Correlation Length and Correlated-Proton Raman Intensity from Amorphous Ice and Supercooled Water up to Dense Supercritical Steam". *Physical Chemistry*. **1995,** 99:11225-11229.

Wang C-Y., Groenzin H., Shultz M. J. "Surface characterization of nanoscale TiO_2 by Sum Frequency Generation using methanol as a molecular probe". *Physical Chemistry B*. **2003**, 108:265-272.

Weber, J.B. "Mechanisms of adsorption of *s*-triazine by clay colloids and factors affecting plant availability" *Residue reviews*. **1970,** 33: 93-129.

Wellhouse G., Bleam W. "Atrazine hydrogen bonding potentials". *Environmental Science and Technology*. **1993,** 27: 494-500.

Wellhouse G., Bleam W. "NMR spectroscopy investigation of hydrogen bonding in atrazine". *Environmental Science and Technology*. **1992**, 26: 959-964.

Windholz, M. The Merck Index: an encyclopedia of chemicals and drugs. 9th Ed. Merck Rahway, NJ, **1976**.

Worrall F., Parker A., Rae J., Johnson A. "Equilibrium adsorption of isoproturon on soil and pure clays". *European Journal Soil Science***. 1996,** 47: 265-272.

Worthing C., Walker B. The Pesticide manual: a world compendium**.** Croydon. British Crop Protection Council. England, **1983**.

Yang M., Chou K., Somorjai G. “The structures and reactions of linear and cyclic C_6 hydrocarbons adsorbed on the Pt (111) Crystal Surface studied by Sum Frequency Generation Vibrational Spectroscopy: Pressure, Temperature, and H_2 coadsorption effects”. *Physical Chemistry B*. **2004**, 108:14766-14779.

Zaki M. L., Hasan M. A., Al-Sagheer F., Pasupulety L. “In situ FTIR spectra of pyridine adsorbed on SiO_2-Al_2O3, TiO_2, ZrO_2 and CeO_2: General considerations for the identification of acid sites on surfaces of finely divided metal oxides”. *Colloidal surfaces*. **2001**:190: 261-270.

Zaki M. L., Hasan M. A., Al-Sagheer F., Pasupulety L. “Surface chemistry of acetone on metal oxides: IR observation of acetone adsorption and consequent surface reaction on silica-alumina versus silica and alumina”. *Langmuir*. **2000**, 16:430-435.

Zeroka D., Jensen J. “Infrared spectra of some isotopomers of methylamine and the methylammonium ion: a theoretical study”. *Journal of Molecular structure (Theochem)*. **1998**, 425:181-192.

Zeroka D., Jensen J., Samuels A. “Infrared spectra of some isotopomers of ethylamine and ethylammonium ion: a theoretical study”. *Journal of Molecular structure (Theochem)*. **1999**, 465:119-139. (I)

Zeroka D., Jensen J., Samuels A. “Infrared spectra of some isotopomers of Isopropylamine: a theoretical study”. *International Journal of Quantum Chemistry*. **1999**, 72:109-126. (II)

Zhang D., Guttow J., Eisenthal K. “Vibrational spectra, orientations, and phase transitions in log-chain amphiphiles at the air-water interface: probing the head and tails groups by Sum Frequency Generation”. *Journal Physical Chemistry*. **1994**, (98): 13729-13740.

Zhang Z. Z., Low P., Cushman J., Roth C. “Adsorption and heat of adsorption of organics compounds on montmorillonite from aqueous solutions”. *Soil Science Society of America*. **1990,** 54:59-66.

Zhuravlev L. T. “The surface chemistry of amorphous silica. Zhuravlev model”. *Colloidal surfaces*. **2000**, 173, 1-45.

APPENDIX A

OPTIMIZATION AND CALIBRATION OF THE LASER VISION OPG/OPA SYSTEM

I. Optimization of the first stage

The purpose of the optimization is to obtain the maximum energy possible from the output beams of the first stage of the Laser Vision OPG/OPA system. The first stage is also called the 532 nm stage since only this laser beam is involved in the creation of the idler and signal beams.

1. Block the pump laser, the 1064 nm laser beam coming into the OPG/OPA.

2. Decrease the output laser energy to ~ 3 mJ.

3. Remove the silica filter that blocks the 532 nm laser beam coming out from the first stage (Figure A.1). This silica filter is mounted in a holder that has a metal part at the back as is shown in Figure A.2. When replacing the silica filter, be sure not to block the idler beam with the metal.

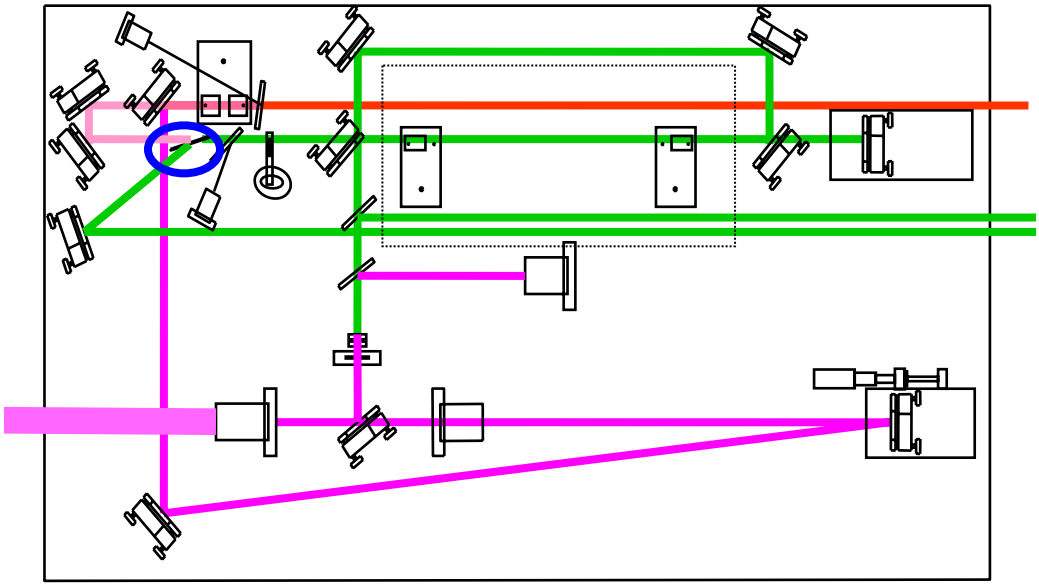

Figure A.1. Schematic OPA/OPG Layout. The silica filter position is circled.

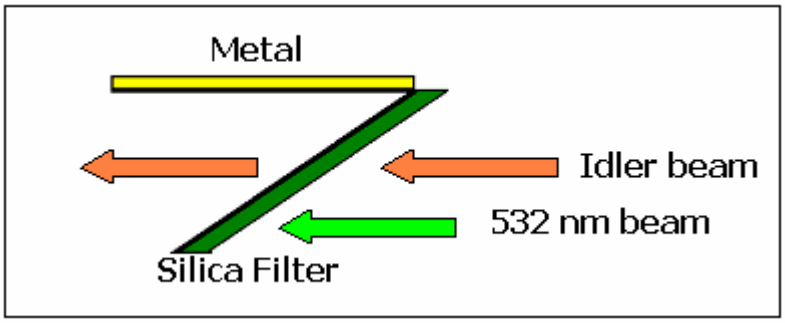

Figure A. 2. Silica filter position on the holder

4. Place a photodiode in the silica filter post holder. Be certain that the 532 nm beam is directed to the detection area on the photodiode. The photodiode needs a filter to absorb most of the 532 nm beam (e.g. Schott color glass filter OG 570) (Figure A.3).

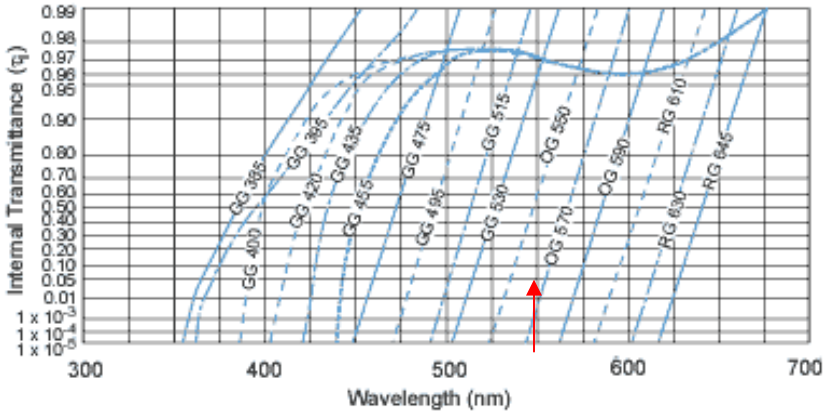

Figure A.3.Filter Graph of a color glass filter OG 570. Courtesy of Schott Glass Technologies, Inc

4. Block the 1064 nm beam in the delay pathway (Figure A.4).

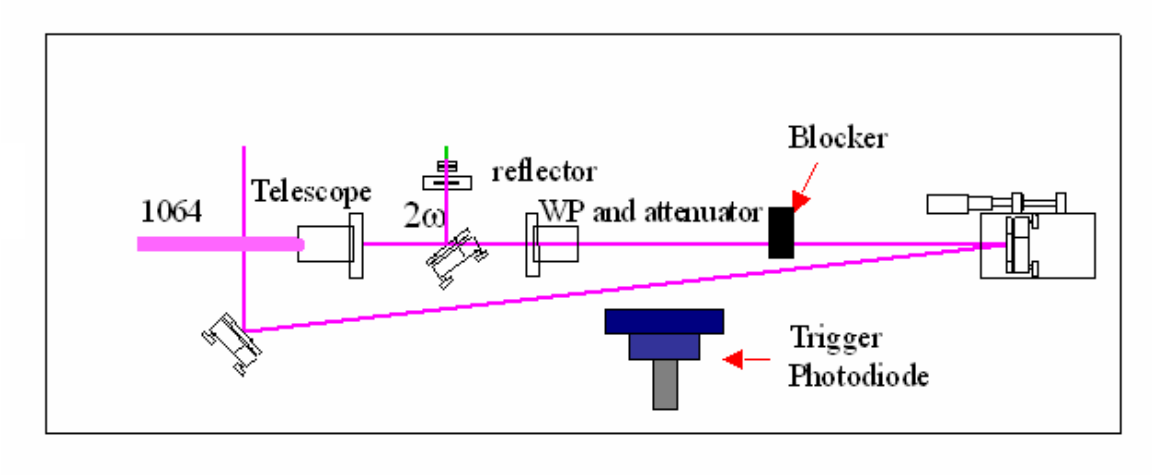

Figure A.4. Schematic of the trigger photodiode position on the 1064 nm delay pathway.

5. Place a second photodiode close to the 1064 nm delay pathway. This photodiode will be used as trigger as is shown in Figure A.4.

6. Both photodiodes are connected to an oscilloscope. (Move the position of the photodiode to trigger the oscilloscope) Figure A.4.

7. The photodiode used for the signal is plugged into channel 1 whereas the photodiode used as trigger is 2 connected to channel 2. The scale used on the x-axis is ns and mV for the y-axis. The image is obtained after averaging 16 scans.

8. Unblock the pump laser, the 1064 nm laser beam coming into the OPG/OPA and increase the laser energy to 45 mJ.

9. Use the Master Control window and go to 817.8nm (Crystal #1 and Crystal #2 should be phasematching or at least close).

10. Move the position of motor #2 to the red or blue at a base speed of 4 $cm^{-1}sec^{-1}$ to scan faster for a high energy value on the oscilloscope screen. Tune the motor position at a lower (1 $cm^{-1}sec^{-1}$) base speed to obtain the maximum energy value.

11. To save the motor positions open a Notepad file called "Motor parameters", record the date and process you are performing, and save the file. Close the file. Click F4 and a window to record the wavelength will appear. The motor positions will be saved automatically.

12. Repeat the optimization procedure from 740 to 840 nm range in 5 nm increments.

13. In an Excel spreadsheet, plot a graph with the wavelength obtained on the calibrated CCD minus 790 on the "x" axis, and the motor position of motor #2 on the "y" axis to obtain a 6th order polynomial equation (e.g. Table A.1). The polynomial equation should have six decimal places.

Wavelength (nm) (Calibrated CCD)	Wavelength (nm) minus 790 "x" value	Motor Position "y" value
753.12	-36.88	-7230
757.85	-32.15	-6544
762.71	-27.29	-5868
767.66	-22.34	-5199
772.772	-17.228	-4538
777.79	-12.21	-3880
782.9	-7.1	-3226
787.83	-2.17	-2576
792.69	2.69	-1924
797.55	7.55	-1270
802.46	12.46	-613
807.47	17.47	48
812.47	22.59	712
817.9	27.9	1379
823	33	2040
828	38	2695
832.47	42.47	3333
836.22	46.22	3943

Table A.1 Wavelength values and motor positions to obtain a sixth order polynomial equation.

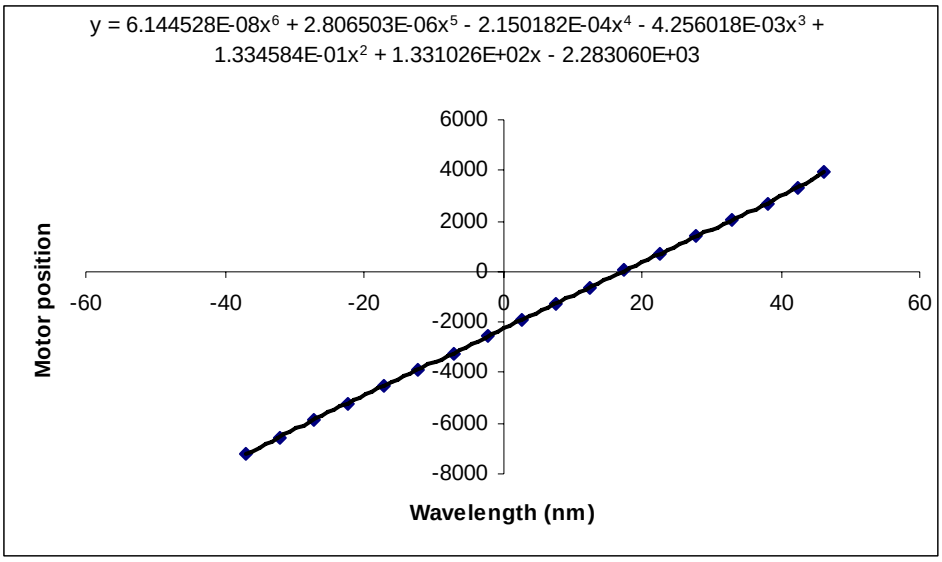

Figure A.5. Plot of the wavelength versus the motor position used to obtain the sixth order polynomial equation.

14. The six coefficients correspond to the values C6, C5, C4 …until C0. These coefficients are imported to MIDIR and BACKUP files. Make sure to keep the same format (e.g. spaces, number of digits), otherwise the program will not recognize the format. (e.g. of MIDIR and BACKUP format in Table A.2.)

Motor #2		
L0	7.900000E+002	0.
C0	-2.515014E+003	0.
C1	+1.358158E+002	0.
C2	-7.700707E-003	0.
C3	-2.846433E-003	0.
C4	+1.700202E-005	0.
C5	+8.023427E-007	0.
C6	-7.278045E-009	0.
C7	+0.000000E+000	0.
C8	+0.000000E+000	0.
C9	+0.000000E+000	0.

Table A.2. Format of the data in the MIDIR and BACKUP files.

15. Proceed with the calibration of the first stage.

II. Calibration of the first stage (Crystal #1)

To have a rough idea if the calibration from the first stage is optimized use the Master Control window and go to 817.8 nm. Decrease the output laser energy to ~ 3 mJ and look at the crystal positions in the OPA/OPG. At this wavelength Crystal #1 is close to normal incidence of the beam. Crystal #1 and Crystal #2 should be phasematching or at least close to as is shown in Figure A.6.

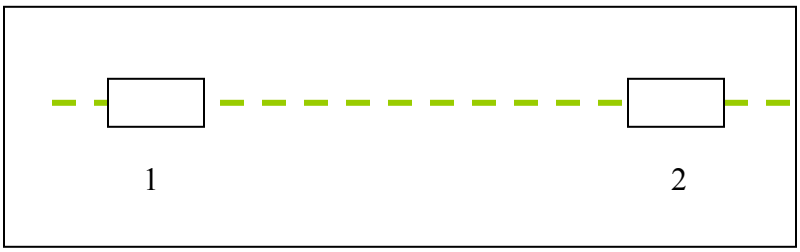

Figure A. 6.Schematic of the Crystal #1 and #2 positions at normal incidence of the 532 nm laser beam.

1. If the Crystals are not close to the normal incidence, block the pump laser, and 1064 nm laser beam coming into the OPG/OPA.

2. Remove the silica filter that blocks the 532 nm laser beam coming out from the first stage. Read item 3 on the optimization of the first stage procedure.

3. Place a fiber optic (sensitive to 700-860 nm radiation) in the holder where the silica filter was.

4. Unblock the pump laser, and the 1064 nm laser beam coming into the OPG/OPA.

5. Block the 1064 nm beam in its delay path (Figure A.7).

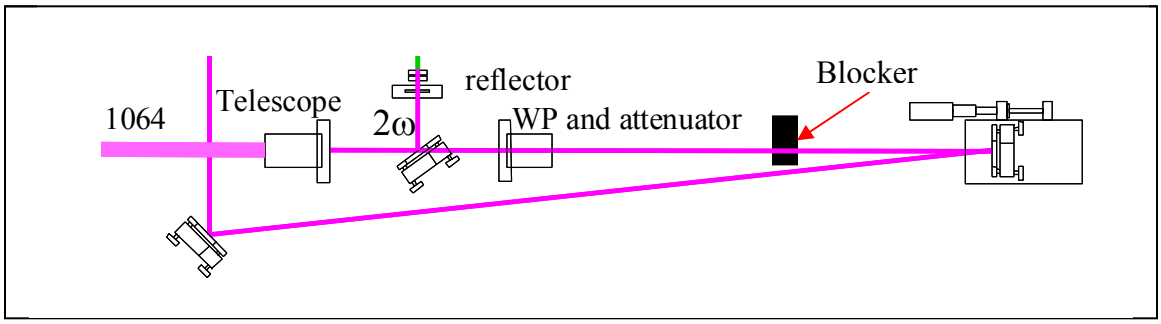

Figure A.7. Delay pathway of the 1064 nm laser beam.

6. Look for if 532 nm laser beam is directed to the fiber optic surface.

7. Increase the laser energy to ~45 mJ. In the detection system (CCD) look for the signal of the 532 nm beam. Adjust the angle of the fiber optic to obtain the highest intensity. The CCD should be previously calibrated using a grating that is efficient for the region from 700 to 900 nm. The grating with 600 g/mm at 1 μm blaze wavelength (Spectra-Physics) shows efficiency above 80% (Figure A.8).

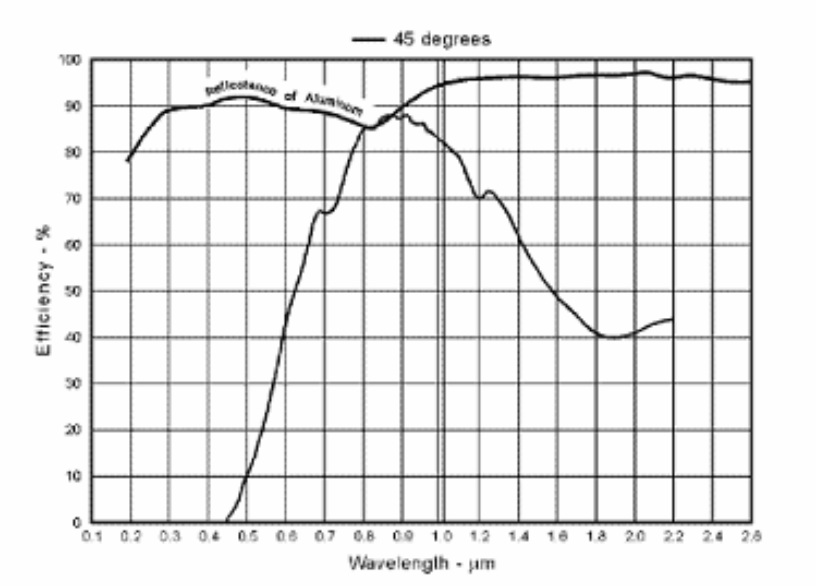

Figure A.8. Diffraction Grating Datasheet. Curve courtesy of Spectra-Physics.

7. Once the highest signal from the 532 nm beam is obtained, look for the signal from 740 to 840 nm beams. Center the monochromator at 780 nm in the calibrated CCD. By using the Master Control go to 780 nm, record the actual wavelength obtained in the CCD, the wavelength at the Master Control (e.g. 780.002 nm) and the motor position of Crystal #1.

8. To save motor positions open a Notepad file called "Motor parameters" record the date and process you are performing and save the file. Close the file. Click F4 and a window to record the wavelength will appear. The motor positions will be saved automatically. Open the "Motor parameters" file to check if the wavelength was saved.

9. Repeat the same procedure of recording wavelengths and motor positions from 740 to 840 nm by using increments of 5 nm. Move the monochromator to the center of the window for each wavelength analyzed.

10. In an Excel spreadsheet, plot a graph with the actual wavelength minus 790 on the "x" axis, and the motor position of motor #1 on the "y" axis to obtain a 6th order polynomial equation. The polynomial equation should have at least 6 decimal places. (For an example look items 13 and 14 in the Optimization of the First Stage).

11. The six coefficients correspond to the values C6, C5, C4 …until C0. These coefficients are imported to MIDIR and BACKUP files. Make sure to keep the same format (e.g. spaces, number of digits), otherwise the program will not recognize the format. (For an example look items 13 and 14 in the Optimization of the First Stage).

12. Using the Master Control window go to 780 nm and check the motor position that was obtained before importing the polynomial equation (for confirmation purposes go to 780 nm and check the peak position in the calibrated CCD).

III. General optimization

The purpose of this optimization is to obtain the maximum of IR energy possible at the IR outlet outside of the OPA/OPG.

1. Using the Master Control window go to 780 nm.

2. Move position of motor #2 to obtain the maximum energy, then move the position of motor #3. Obtain the highest value of energy, and move the position of motor #4 (do not move the position of motor #1). Be certain that the base speed of all the motors is 1 $cm^{-1}sec^{-1}$.

3. Repeat the same procedure of moving the motor position of motor #2, #3, #4 to obtain the maximum energy possible.

4. Once the highest energy value is obtained save the motor positions (for details about this and the following items read items 10, 12, and 13 in the Optimization of the First Stage procedure).

4. Obtain the maximum energy at different wavelengths covering a range from 740 to 840 nm by using increments of 5 nm.

5. Obtain the six-order polynomial equations for each of the motors (except motor #1)

6. Import the equations to MIDIR and BACKUP files.

APPENDIX B

ALIGNMENT OF THE LASER VISION OPG/OPA SYSTEM

1. Reduce the pump laser output ~ 3 mJ.

2. Wear protective eyeglasses (for 532 nm, 1064 nm and infrared radiation).

3. Block the 1064 nm laser beam coming into the OPG/OPA.

I. Alignment of the first stage (532 nm stage)

1. Remove Crystal #1 and Crystal #2 and use their posts as position reference points (record the orientation of the crystals, since each crystal has a particular face facing the incoming beam) Figure B.1.

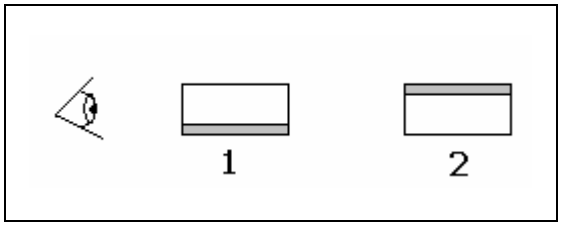

Figure B.1. View of Crystal #1 and Crystal #2 layout from left to right starting at the pump input side.

2. The 532 nm beam must be positioned just above the metal posts that hold the crystals, as is shown in Figure B.2.

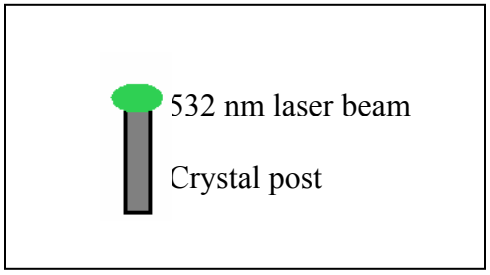

Figure B.2. Side view of the 532 nm laser beam on the metal post.

3. The pathway of the 532 nm laser beam coming into the stage is shown in Figure B.3.

4. Block the amplification pathway on Mirror C and remove Mirror E (Figure B.3).

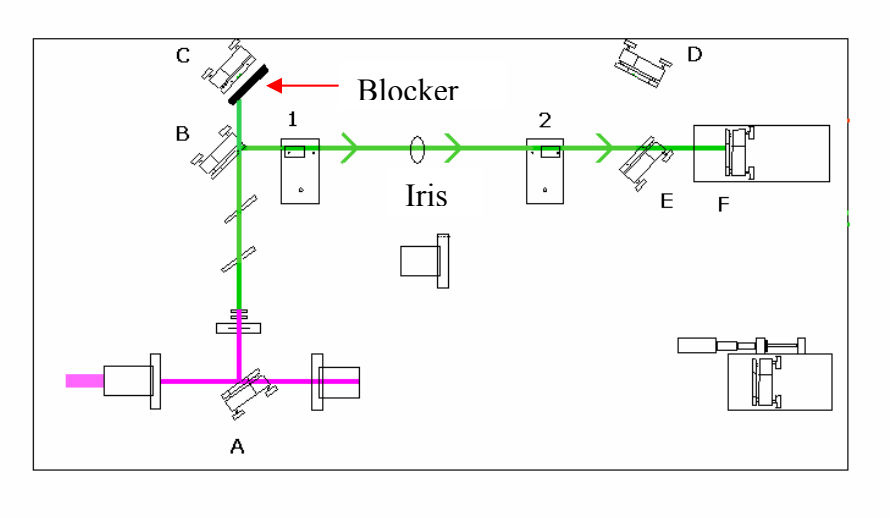

Figure B.3. Generation pathway of the 532 nm laser beam in the first stage of the OPG/OPA

5. To adjust the position of the 532 nm laser at the post of Crystal #1, tweak Beam Splitter A.

6. To adjust the beam position on the post of Crystal #2, tweak Beam Splitter B.

7. Look for the retroreflected beam at the iris, and on Beam Splitter B. The reflected beam should be one beam on Beam Splitter B. If some adjustments are necessary tweak the Retro Reflecting Mirror F on the translation stage.

8. Put Mirror E back.

9. The amplification pathway is shown in Figure B.4.

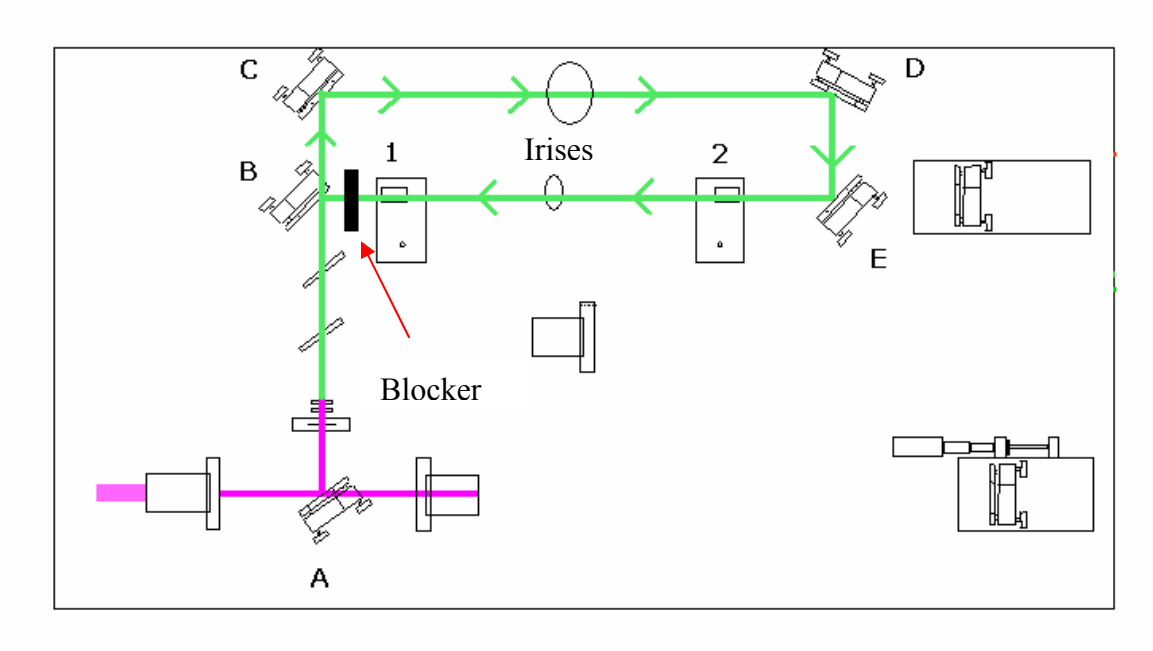

Figure B.4. Amplification pathway of the 532 nm laser beam on the first stage on the OPA/OPA.

10. Block the generation pathway of the 532 nm laser beam as is shown in Figure B.4.

11. To adjust the position of the 532 nm laser beam on Crystal #2 move Mirror D

12. To adjust the position of the 532 nm laser beam on Crystal #1 move Mirror E.

13. Check if the beams are overlapped on Beam Splitter B by partially blocking the beam with horizontal movements.

II. Alignment of the second stage (1064 nm stage)

1. Remove the silica filter, the dichroic filter that removes the residual 532 nm laser beam, and the dichroic filter that removes the 1064 nm residual beam (Figure B.5). The 532 nm laser beam will be used as reference.

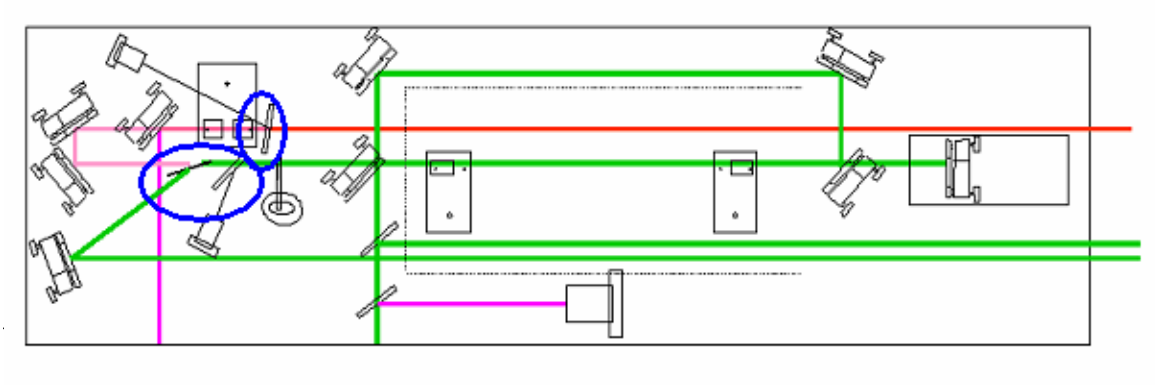

Figure B.5.Silica filter and dichroic filters location.

2. Remove the stack of polarized plates located just before the infrared outlet.

3. Block the 1064 nm laser beam in its delay pathway to the second stage, as is shown in Figure B.6.

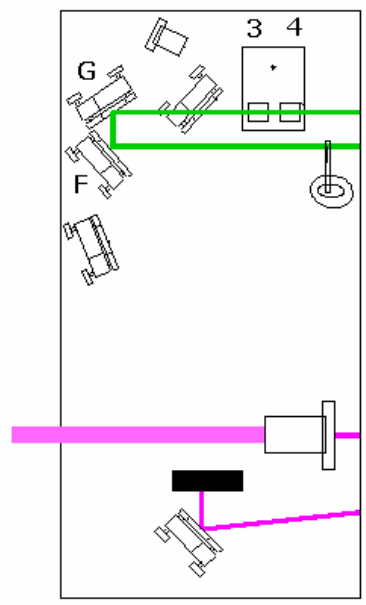

Figure B.6. Pathway of the blocked 1064 nm laser beam before entering to the second stage.

4. Remove Crystal #3 and Crystal #4, Fig. B.6. Record the orientation of the crystals, since each crystal has a particular face facing the incoming beam.

5. Use the software to rotate one of the crystals ~ 90 degrees for better access to the screws.

6. The 532 nm laser beam will be used as a reference. Two beams reaching Mirror F will be observed. To determine which 532 nm beam will be used as reference, look for the residual 532 nm laser beam on the back of Beam Splitter B. This beam will not be used as reference.

7. To adjust the position of the 532 nm laser on the posts of Crystal #3 and Crystal #4, move Mirror F, Fig. B.7.

8. To adjust the position of the 532 nm laser on the post on the empty Crystal Stage H, move Mirror G, Fig B.7.

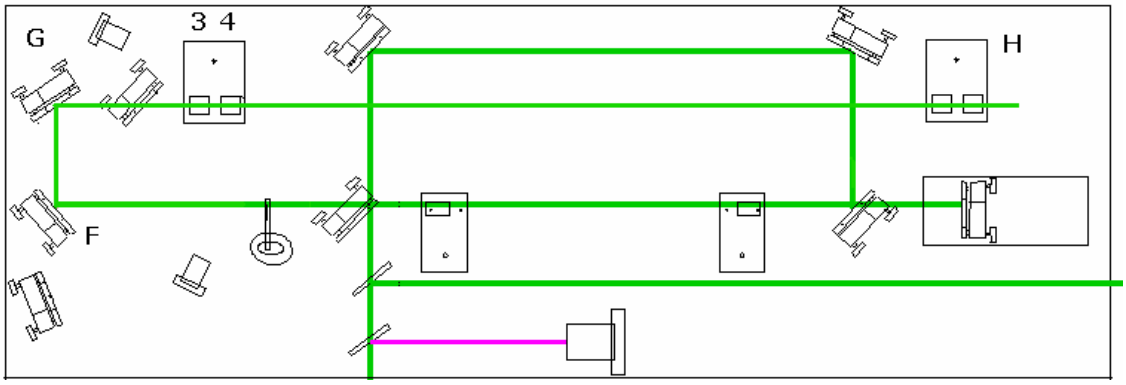

Figure B.7. Location of the empty Crystal Stage H.

9. Block the 532 nm laser beam and unblock the 1064 nm laser beam that enters on the second stage (Figure B.8).

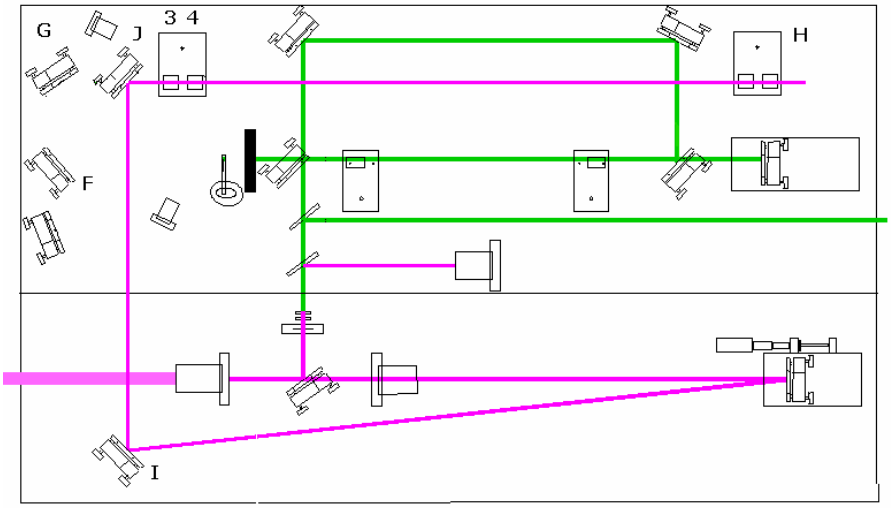

Figure B.8. Pathways of the 1064 nm laser beam entering in the second stage and the 532 nm laser beam blocked outside of the first stage.

10. Adjust the position of the 1064 nm laser beam on the posts of Crystal #3 and Crystal #4 by moving Mirror I.

11. To adjust the position of the 1064 nm laser beam on the empty Crystal Stage H move the dichroic Mirror J.

12. Unblock the 532 nm laser beam and ensure that it overlaps with the 1064 nm laser beam on the posts of Crystal #3 and Crystal #4.

13. Replace the silica filter, the dichroic filter that removes the residual 532 nm laser beam, the dichroic filter that removes the 1064 nm residual beam, and the stack polarized plates.

14. Block the pump laser and the 1064 nm laser beam inlet to OPG/OPA.

15. Replace Crystal #3. Be certain that the orientation of the crystal is correct.

16. Replace Crystal #4. Place the crystal perpendicular to the incoming beam and then use the Master Control to move the position until Crystal #3 and Crystal #4 are close to phasematching.

17. Replace Crystal #1 and Crystal #2, making certain that the orientation of the crystals is correct.

18. Unblock the pump laser, and decrease the output energy to ~ 3 mJ.

19. Look for the back reflection beam when tightening the screws. The reflected light will be either higher or lower than the incoming beam.

20. The back reflection beam from Crystal #2 can be seen on the iris located in the first pass of the first stage.

21. The back reflection beam from Crystal #1 can be seen on the Beam Splitter B.

22. Using the Master Control go to 817.8 nm. At this wavelength Crystal #1 is close to normal incidence of the beam.

23. Reset the motor positions for Crystal #1 and Crystal #2 to zero.

24. Close out all motor control except for Crystal #1 and Crystal #2.

25. Remove the silica filter and place a photodiode connected to an oscilloscope to look for the maximum energy from the first stage by moving position of motor #2. (For details on how to set up a photodiode, read items 3 to 8 in the optimization of the first stage procedure). (For details on how to set up a fiber optic read items 2 to 7 in the calibration procedure).

26. Once the maximum energy from the first is obtained remove the fiber optic and replace the silica filter.

27. Open the control windows for motors #3 and #4.

28. Crystal #3 and Crystal #4 should be at normal incidence to the incoming beam.

29. Reset the motor positions of Crystal #3 and Crystal #4 to zero.

30 Using the computer control for each of the crystals on motor #3 and #4, rotate each until the positions read +5585 for motor #3 and –5283 for motor #4. These positions are approximate, but should be very close to the values required for phasematching when the crystals in the first stage are at normal incidence.

31. Proceed with the calibration of motor #1, the optimization of the first stage, and finally the general optimization procedures.

32. Obtain an IR profile by scanning from 2600 to 4000 cm^{-1} with a 2 sec integration time and a step size of 10 cm^{-1}.

33. Obtain a spectrum of polystyrene attached to the infrared outlet.

34. The alignment outside the OPG/OPA should be completed.